ULTRA-SENSITIVITY OF CELL ADHESION IN A MECHANICALLY HETEROGENOUS ENVIRONMENT

by

Mehdi Roein-Peikar

A dissertation submitted to Johns Hopkins University in conformity with the requirements for the degree of Doctor of Philosophy

Baltimore, Maryland

May, 2016

ABSTRACT

Cell adhesion regulates critical cellular functions in adherent cells. Yet, the fundamental mechanism during the early events in cell adhesion remains unclear. At the most elementary level, cell processes its environment using single molecular clues for its decision making. Herein, we utilized our recently developed DNA tether called tension gauge tether (TGT) to study the mechanical requirements of integrin-mediated cell adhesion. Our lab showed that cells need to experience a threshold force of 40 pN through single integrin-ligand bonds to initiate adhesion and spreading. We also demonstrated that just a few copies of strong (~ 54 pN) TGTs per cell are enough for cell adhesion and spreading as long as there is a high density of weak tethers. Additionally, we showed that 12 pN and 23 pN tethers, which are unable to induce cell adhesion individually, can induce cell adhesion if they are presented together to the cell. Therefore, the cells appear to be able to perform relative force measurements instead of absolute force measurements. Furthermore, we show by direct single molecule imaging that a cell needs only two copies of 23 pN tethers for such relative force measurements. Moreover, we found that such an observation is due to the presence of relatively stronger tethers that act as membrane holders, which

keep the cell membrane close to the surface. Therefore, relatively stronger tethers allow the weaker tethers that are ruptured to re-anneal and subsequently cells remain adhered to the surface.

Readers: Dr. Taekjip Ha

Dr. Jungsan Sohn

ACKNOWLEDGEMENTS

First and foremost, I would like to acknowledge Dr. Taekjip Ha, with whom I have enjoyed the pleasure of working with for the past few years. Under his guidance I completed this work and, in the process, he helped me to develop the skills I needed to become an independent researcher. I would also like to acknowledge Dr. Qian Xu, with whom I have worked very closely and collaborated with for more than a year and learned a lot.

Additionally, I want to acknowledge all the postdocs in my lab who are now faculty members in different parts of the world and this entire group provided an invaluable source of inspiration for me to pursue science: Professor Xuefeng Wang, Professor Farhan Chowdhury, Professor Jingyi Fei, Professor I-Ren Lee, Professor Hajin Kim, Professor Isaac Li and Professor Kyu Young Han.

I cannot say enough about the positive environment that I experienced while working in Professor Taekjip Ha, Professor Sua Myong lab and Professor Rong Li lab. Whether it was a search for a crucial reagent or just somebody to help in moving from Illinois to Maryland, there always seemed to be someone willing to lend a hand. I would like to thank the past and current postdocs and graduate students: Dr. Benjamin Leslie, Dr. Byoung Choul Kim, Dr. Hye Ran Koh, Dr. Aakash Basu, Dr. Xinghua Shi, Dr. Reza Vafabakhsh,

Dr. Sultan Doganay, Dr. Thuy Ngo, Dr. Salman Syed, Dr. Seogjin Park, Dr. Sinan Arslan, Sangwoo Park, Vasudha Aggarwal, Chang-Tin Lin, Anustup Poddar, Olivia Yang, Boyang Hua, Digvijay Singh, Jaba Mitra, Jichuan Zhang, Amir Hossein Ghanbari Niaki, Tunc Kayikcioglu, Dr. Peggy Qui, Jim Lee, Dr. Ram Tippana and Dr. Hui-Ting Lee.

I also want to acknowledge Professor Rong Li, Professor Martin Schwartz, Professor Claire Waterman and Professor Ning Wang for helpful discussions and suggestions which improved my research project dramatically. Finally, I would like to thank Elizabeth (Betty) Ujhelyi in University of Illinois at Urbana-Champaign and Kelsey Williams in Johns Hopkins School of Medicine for helping and providing the reagents for my research.

I would like to give special thanks to my friends in University of Illinois at Urbana-Champaign and Johns Hopkins School of Medicine for listening, offering me advice, and supporting me through this entire process. Special thanks to James Wratten, Farshid Jafarpour, Rezvan Shahoei, Tatyana Perlova, Courtney Byard, Bo Han, Renato Mancuso, Neriman Tokcan, Sina Khazali, Sam Hamedi, Jackson Fliss, Dalmau Reig, Mathew Lapa, David Meldgin, Reuven Birnbaum, Emily Schlafly, Alexandre Zakjevskii and Shiva Razavi.

I would like to end by thanking my family members for their love and support. I would especially like to thank my father and mother, Reza and Afsar, and also my sisters, Mandana and Mitra. I know that I would not have the spark of curiosity inside of me had I not been in a family that encourages me to keep the hunger for learning. As I sat here thinking about where the root of my interest in science began I came to realize that if not for the persistence of my parents in trying to teach me and my siblings about the world we would not be where we are. I also would like to thank my uncle, Khosrow Moadeli who supported me when I decided to study physics. Finally, I would like to thank my adviser during my residency in Shiraz Dental School, Dr. Parisa Salehi whom I know and respect as my mother. My only hope for the future is that I can eternally return my family the favor.

Sincerely,

Mehdi Roein-Peikar

TABLE OF CONTENTS

ABSTRACT ii

ACKNOWLEDGEMENTS iv

TABLE OF CONTENTS vii

TABLE OF FIGURES ix

Chapter 1 1

INTRODUCTION 2

RESULTS AND DISCUSSION 7

Multiplexing weak and strong TGTs 7

Multiplexing transforms how the cells treat the weak tethers 8

Multi-variable single cell analysis 10

Multiplexing leads to ultra-sensitivity for strong TGT 12

Chapter 2 36

INTRODUCTION 37

RESULTS AND DISCUSSION 40

Cell adhesion is supported on a multiplexed weak TGT surface 40

Ultrasensitivity of cells to single molecules 42

Similarity between 54 pN, 12 pN & 23 pN and PnP surfaces 44

23 pN TGTs form supporting membrane holders to endorse cell adhesion 46

DISCUSSION 48

METHODS 51

Cell Culture 51

Fabrication of tension gauge tether (TGT) 52

Preparing the surfaces 52

Preparation of cell solution 52

Incubation of the cells on the surface, fixation and imaging 53

Image Analysis 53

FAK activation assay 55

Single Molecule Experiment 55

REFERENCES 88

CURRICULUM VITAE 100

TABLE OF FIGURES

Chapter 1

Figure 1. 1 21

Figure 1. 2 23

Figure 1. 3 25

Figure 1. 4 27

Figure 1. 5 29

Figure 1. 6 32

Figure 1. 7 34

Chapter 2

Figure 2. 1 57

Figure 2. 2 59

Figure 2. 3 62

Figure 2. 4 64

Figure 2. 5 67

Figure 2. 6 70

Supplementary Figure 2. 1 72

Supplementary Figure 2. 2 74

Supplementary Figure 2. 3 76

Supplementary Figure 2. 4 78

Supplementary Figure 2. 5 80

Supplementary Figure 2. 6 82

Supplementary Figure 2. 7 84

Supplementary Figure 2. 8 86

Chapter 1

Ultrasensitivity of cell adhesion to the presence of mechanically strong ligands

INTRODUCTION

Research into how cells sense and respond to mechanical cues in their environments has shown that the processes of growth, motility and development are strongly influenced by the mechanical properties of cellular surroundings. Most of these studies have measured the cell's macroscopic, ensemble-averaged response to forces exerted between receptors and their ligands which mediate mechanical communication (Engler et al., 2006; Hoffman et al., 2011; Ingber, 2006; Oakes and Gardel, 2014; Watt and Huck, 2013). Relatively few studies have quantified these actions at the molecular level (Gordon et al., 2015; Grashoff et al., 2010; Jurchenko et al., 2014; Liu et al., 2013; Morimatsu et al., 2013; Morimatsu et al., 2015; Stabley et al., 2012; Zhang et al., 2014). Yet, at the most elementary level, the sensing of the mechanical environment must be performed by single molecules in mechanical contact with the environment, and the cell then must be able to process the single molecular events for its decision making.

One of the best characterized cellular mechanical processes is adhesion to the extracellular matrix (ECM) – the microenvironment of animal cells (Dobereiner et al., 2004; Evans and Calderwood, 2007; Halder et al., 2012; Watt and Huck, 2013). The membrane-bound receptor proteins called

integrins interact with the ECM and relay information about the extracellular environment to the cell interior and to the underlying actin cytoskeleton through interaction with other proteins (del Rio et al., 2009; Fraley et al., 2010; Friedland et al., 2009; Grashoff et al., 2010; Guan, 1997; Koo et al., 2002; Parsons et al., 2010; Sawada et al., 2006; Wang et al., 2005). The spatial extent of the ECM communication with the actin cytoskeleton through integrins ranges from nano to micrometers with a force sensitivity which ranges from a few pico-Newton (pN) to a few hundreds of pN (Blakely et al., 2014; Cavalcanti-Adam et al., 2007; Jiang et al., 2003; Kim et al., 2015; Lehenkari and Horton, 1999; Stabley et al., 2012; Tan et al., 2003; Wang et al., 1993). Precise understanding of the underlying mechanisms requires techniques which are sensitive in these ranges.

To investigate the single molecular forces involved in mechanical processes in cells, we developed a technique called tension gauge tether (TGT) (Wang and Ha, 2013). This technique leverages the well-understood rupture dynamics of short, double-stranded (ds) DNA, which was previously used to determine the antibody-antigen binding forces (Albrecht et al., 2003), in order to determine the magnitude of forces across a single receptor-ligand bond required for triggering certain cellular behaviors, for example integrin-mediated cell adhesion (Chowdhury et al., 2015; Wang and Ha, 2013), Notch

signaling activation (Cocco et al., 2001) and immune cell activation (Wan et al., 2015). In a TGT designed for integrins, one strand, termed the top strand, is covalently linked to the RGDfK ligand which is a short peptide mimic of the ECM (Takada et al., 2007), and the other strand (bottom strand) is covalently linked to a biotin [Fig 1.1]. The dsDNA is then tethered to a polymer-passivated glass surface through biotin. By keeping the location of the ligand fixed while shifting the location of the biotin progressively away from the ligand, the force required to rupture the dsDNA increases in a quantifiable fashion.

During the cell adhesion process any bond formed between an integrin and a ligand is thought to be subject to a mechanical force or tension. Several different mechanisms may contribute to this tension, including an active force arising from intracellular processes and a generic physical force associated with the cell membrane. If this force across a single integrin-ligand bond required to initiate stable cell adhesion is greater than the tension tolerance (T_{tol}) of the tether, the top strand engaged with an integrin is removed from the surface by the cell-induced rupture of dsDNA. This can be detected as a loss-of-fluorescence from the surface if the top strand is labeled with a fluorophore. On the other hand, if the required force is smaller than T_{tol}, the integrin will continue to engage with the RGDfK and mediate cell adhesion

and spreading. Regardless of how a single integrin is coupled to the membrane, the underlying cytoskeleton, and to other integrins, the force applied to our DNA tether is applied through a single integrin-ligand bond.

The physics behind short (< 20 base pairs) dsDNA rupture was originally described by P.G. de Gennes (de Gennes, 2008) and has since then been experimentally verified (Hatch et al., 2008). The equation for the rupture force is the following:

$$T_{tol} = 2f_c[x^{-1}\, tanh\left(\frac{xl}{2}\right) + 1] \qquad (1)$$

where T_{tol} is the rupture force, f_c is the breaking force of a single base pair, x is related to the spring constant of DNA and l is the number of base pairs (bp) between the points of force application on the two complementary strands of DNA. In our case, l represents the number of bp separating RGDfK and biotin [Fig 1.1 inset]. Using magnetic tweezers, the Prentiss group determined the values for x^{-1} and f_c to be 6.8 bp and 3.9 pN, respectively(Hatch et al., 2008). On a DNA with a total length of 18 bp, when the RGDfK and biotin are placed closest to each other (l = 1 bp), T_{tol} is ~ 12 pN whereas T_{tol} is ~ 54 pN when the biotin is placed farthest away from RGDfK (l = 18 bp). Because the magnetic tweezers experiments that yielded the parameters to the de Gennes

model were performed by increasing the force incrementally after 1 or 2 seconds of constant force did not rupture the DNA, T_{tol} values we estimate should be considered only approximate. The absolute force values may be different from our estimates if the cellular time scale of force application is much longer or shorter than 1 to 2 seconds.

Prior TGT studies revealed the tension threshold for integrin-mediated cell adhesion to be ~ 40 pN (Wang and Ha, 2013) . In these experiments, TGT with nine different T_{tol} values ranging from 12 pN to 54 pN were individually presented to cells. After a 30-minute incubation, cells did not adhere stably to the surface if TGT with $T_{tol} < 43$ pN was used. On the other hand, cells adhered stably if TGT with $T_{tol} \geq 43$ pN was used. The tension threshold appeared universal across several different cell types, both cancerous and noncancerous (Chowdhury et al., 2015; Wang and Ha, 2013) and was shown to hold as early as the first five minutes of adding the cells to the TGT-coated surface (Wang and Ha, 2013). This 40 pN force across a single bond outside the cell may contribute to the range of single molecule forces, 5 pN - 25 pN, proposed to be experienced by the intracellular proteins that bridge integrins to the actin cytoskeleton (del Rio et al., 2009; Grashoff et al., 2010; Rognoni et al., 2012; Yao et al., 2014).

The ECM is complex, presenting a great variety of ligands with which integrins can interact. Our objective in this work was to better approximate this complexity and extend the prior work which quantified cellular response to only one tether strength at a time. By presenting both weak (T_{tol} ~ 12 pN) and strong (T_{tol} ~ 54 pN) tethers to cells simultaneously in a scheme we call "TGT multiplexing (MP)" [Fig 1.1], we could study cell mechanics at the molecular level in an environment more similar to the ECM.

RESULTS AND DISCUSSION

Multiplexing weak and strong TGTs

In the multiplex scheme, weak and strong TGTs are made distinguishable from each other through labeling with fluorophores of different colors, Cy3 and Cy5, respectively. A typical experiment arrays three circular spots of TGT on the same imaging surface, each with an area of ~ 13 mm^2 and a surface density of ~ 400 tethers/μm^2, which mirrors the density of integrins in the membrane of animal cells (40 – 3000 /μm^2) (Wiseman et al., 2004). To achieve these conditions, 3 μL of 1 μM TGT solution is spotted onto a neutravidin functionalized glass surface. After a 10-minute incubation period, unbound TGTs are thoroughly rinsed away.

The first spot presents only the weak TGT and the second presents only the strong TGT. The third spot presents multiplexed weak and strong TGT which are mixed at equi-molar concentrations. Chinese Hamster Ovary (CHO-K1, American Type Cell Culture) cells are cultured on the surface for 30 minutes in a 37 ^{o}C incubator. Afterwards, unbound cells are gently rinsed away and the sample is fixed. Imaging the cells using differential interference contrast (DIC) and epi-fluorescence microscopy (Zeiss 200M Axiovert) allowed us to obtain two main observables from the images: 1) the degree of TGT rupture is reported through loss-of-fluorescence from the imaging surface and 2) the number of cells that remain attached. Very few cells remained attached after gentle washing when only the weak TGT was used whereas a high density of adherent cells was observed with the strong TGT alone or with TGT multiplexing. To ensure that fixation does not bias the results, experiments have been performed using both live and fixed cells. In the context of these two observables, there were no noticeable differences between fixed and live cell images (not shown).

Multiplexing transforms how the cells treat the weak tethers

Fluorescence images from a typical experiment are shown in Figure 2. Similar to what was previously reported (Wang and Ha, 2013), fluorescence images

of the weak TGT-coated surface showed uniformly dark patches about the size of single cells, likely due to the rupture of weak TGTs induced by cellular forces transmitted through integrins when the cell tries to gain foothold by pulling on ligands [Fig 1.2(a)]. Imaging the cells without rinsing confirmed this interpretation because fluorescence loss was observed only under the cells (not shown). Cellular forces that ruptured the weak TGTs are likely provided by actin cytoskeleton instead of passive sources such as membrane repulsion because actin filament inhibitor (1 μM latrunculin A) eliminated fluorescence loss (Fig 1.2A). On the other hand, the strong TGT-coated surface showed lower degrees of rupture, with scattered dark regions localized to the periphery of the contact area between the cell and the surface [Fig 1.2(b)]. The peripheral (or edge) rupture of the strong TGT appears to be caused by an ATP-powered molecular motor, myosin II (Wang et al., 2015). When weak and strong TGTs are multiplexed and presented to cells simultaneously, the cells adhered well to the surface after rinsing as was the case for the strong TGT-coated surface. Unexpectedly, the rupture patterns for the weak TGT changed to become identical to those observed for the strong TGT. That is, instead of the uniformly dark rupture footprint for the weak TGT-coated surface, cells ruptured both tethers on the periphery of the contact area as if they are both strong TGTs [Fig 1.2(c)]. These observations suggest that the

presence of strong tethers can significantly influence how cells sense and act on the weak tethers.

Multi-variable single cell analysis

We further quantified rupture footprint patterns by analyzing more than a hundred cells from each surface in terms of two variables [Fig 1.3(a)]. The first variable is the degree of TGT rupture. This is measured by comparing the fluorescence intensity underneath a cell to a nearby surface without any attached cells. The background, which is measured from an area off of the TGT spot, is subtracted from both values before the comparison. To calculate this, the following formula is used,

$$Rupture\ (\%) = \frac{MF_{surface} - MF_{cell}}{MF_{surface} - MF_{background}} \qquad (2)$$

where *MF* is the mean fluorescence intensity. Values are measured in ImageJ (open-source software developed by the National Institutes of Health) by selecting the corresponding region. For the weak TGT spot, regions were selected directly from the fluorescence images since this surface does not retain cells after rinsing. For the rest of the spots, DIC microscopy was used to image the cells directly. The regions for analysis were selected from these DIC images and the corresponding fluorescence images were analyzed.

Because the analysis of the images from the weak TGT spot is different from the analysis for the other two spots, we performed a control comparison to rule out the possibility of any analytical bias. For the strong TGT, we selected regions in two different ways. First, regions were selected directly from the fluorescence images and the percent rupture was calculated. Second, regions were selected from DIC images and the percent rupture was calculated based on the corresponding fluorescence images. The values for the percent rupture from the two analyses were within standard error of each other: 8.50%± 1.01 and 8.27%±0.99, respectively.

The second variable describes the spatial distribution of the rupture. That is, underneath the cell, does the rupture occur everywhere or is it concentrated to a specific area? As a quantitative measure, we define a rupture moment, *I*, analogous to the moment of inertia from mechanics. A bigger value of *I* represents rupture at the periphery of the contact area underneath each cell, or, "edge rupture". A smaller value suggests that the rupture is more uniformly localized, or, "uniform rupture".

We used the following formula,

$$I = \frac{\sum_{i=1}^{N} M_i R_i^2}{A \sum_{i=1}^{N} M_i} \qquad (3)$$

where A is the area of the cell measured in ImageJ, R_i is the distance from the approximate center of the fluorescence footprint underneath a single cell to the ith pixel, M_i is the percent rupture of the ith pixel as defined in equation (2), and N is the total number of pixels.

A scatter plot of the percent rupture versus I for many single cells [Fig 1.3(a)] shows that weak TGT and strong TGT rupture patterns form two distinct clusters. Cells showed higher rupture percentage and smaller I on the weak TGT-coated surface compared to the strong TGT-coated surface. On the multiplex (MP) surface, the rupture patterns of both weak and strong TGTs cluster together with each other and with that of the strong TGT-coated surface, showing indeed that the presence of strong TGTs transform the way cells treat the weak TGTs. The ensemble average values of rupture percentage and I [Fig 1.3(b)] further support the qualitative observations shown in Figure 2. Taken altogether, cells act on both tethers similarly in MP, showing small percent rupture values and large I values which are characteristics of edge rupture, as if both tethers are strong.

Multiplexing leads to ultra-sensitivity for strong TGT

Up to this point, TGT spots have been prepared with high surface densities so that each cell would have > 200,000 TGT molecules underneath, on average.

This number is estimated from the known surface density given 1 μM incubation concentrations (~ 400 TGT /μm^2) (Chowdhury et al., 2015) and the measured average area of cells attached to the strong TGT and MP spots (~ 600 μm^2). For a point of reference, the aerial footprint of CHO-K1 cells used in our experiments ranges from 80 μm^2 (for the cells that do not adhere to the surface with weak tethers and just leave a fluorescent footprint) to 800 μm^2 (for the cells adhered on the surface with strong tethers).

Here, we define the term, "weak tether transformation" to refer to the shift from the uniform rupture of weak tethers, when presented alone, to edge rupture when the weak is multiplexed with the strong. A question then arises: how many strong tethers are needed for the cell to undergo a weak tether transformation? To answer this question, we progressively lowered the incubation concentration of strong TGT from 1 μM to 0 pM while maintaining the weak TGT concentration during incubation at 1 μM. Cells were cultured on these MP titration spots for 30 minutes, rinsed, fixed and imaged. The images were analyzed, as before, in terms of: 1) the number of cells stably adhered per unit area and 2) rupture pattern (the rupture percentage and *I*). As a control, strong TGT is presented alone to cells over the same range of concentrations.

Figure 4(a) shows representative DIC and fluorescence images of the MP surface obtained with 1 μM weak TGT and 40 nM, 2 pM and 0 pM strong TGT. Very few cells adhered to the surface in the absence of any strong TGT but even at 2 pM strong TGT, 500,000 fold dilution compared to weak TGT, we observed many cells adhering albeit with lower cell counts than in the case of 40 nM strong TGT [Fig 1.4(a) and 4(b)]. In addition, the fluorescence rupture pattern for the weak TGT underneath adhered cells for both 2 pM and 40 nM TGT showed edge rupture, indicating weak tether transformation.

Figure 4(b) shows the plot of adhered cell count. When cells are cultured on the strong TGT-coated surface, only background levels of adhered cells are observed for concentrations lower than 40 nM. However, when weak tethers are present, cells adhered for strong TGT concentration down to 2 pM but not at 0.2 pN. The attached cell count, although well above background levels, decreased on MP titration spots with pM concentrations of the strong TGT. Overall, our data suggest that even at 2 pM incubation concentration, strong TGT can induce weak tether transformation for a subset of cells.

We further analyzed the weak TGT rupture patterns under adhered cells and calculated the rupture percentage and *I* from single cells [Fig 1.5]. At 2 pM and 2 nM incubating concentrations of strong TGTs, although some of the

loss-of-fluorescence footprints show uniform rupture, these footprints do not correspond to adhered cells in the DIC images. Instead, the footprints for adhered cells show edge rupture pattern as quantified through rupture percentage and *I* [Fig 1.5(b)] at strong TGT concentrations of 2 pM or above.

At incubation concentrations ≤ 200 pM, the average surface density of strong TGT in the presence of unlabeled 1 μM of weak TGT can be directly determined using single molecule total internal reflection fluorescence microscopy. From these measurements, we estimated the number of strong TGT per cell as a function of the pM incubation concentrations using 600 μm^2 as the average area of an adhered cell [Fig 1.6(a)]. Note that the surface density of strong tethers is three times lower when they are presented together with weak tethers, probably because weak and strong tethers can compete with each other for a finite number of binding sites on the surface.

According to our calibration, the number of strong tethers at 2 pM incubation is about two molecules per cell, suggesting that, even with the uncertainty in the measurement, the number of strong tethers required for weak tether transformation is in the range of low single digit per cell, possibly down to one strong tether. This ultra-sensitivity for strong tethers is a surprising result. Cells do not adhere to a surface displaying either weak tethers alone or strong

tethers at the pM incubation concentrations. Yet, the presence of just a few strong tethers per cell will induce adhesion if, and only if, the surface is also displaying many weak tethers. We can rule out the possibility that the strong tether distribution is highly uneven, leading to localized "hot spots" that display many tethers, because direct single molecule microscopy measurements revealed no such unevenness (Fig 1.6(b)).

Because the adhered cell count on the MP surfaces with picomolar strong tether concentrations is lower than on those with ≥ 20 nM concentrations of strong tethers [Fig 1.4(b)], we hypothesize that there exists a sub-population of ultra-sensitive cells that can be fully activated by just a few strong tethers, leading to adhesion and spreading. As the amount of strong tethers is increased from 2 pM to 2 nM, the adhered cell count is unchanged because only ultra-sensitive cells adhere. At ≥ 20 nM, cell attachment count increases because the less sensitive cell population is then activated.

In summary, we report synergistic mechanical forces in cellular adhesion using TGT multiplexing. Multiplexing a strong tether with a weak tether resulted in two surprising observations. First, the way cells sense and treat the weak tether is transformed in the multiplex scenario: cells treat both TGTs the same, as if the weak tether were strong. And second, cells adhere to a MP spot

when merely a few single molecules of the strong tether are present per cell, as long as there are also many weak tethers.

Although there is a precedent for ultra-sensitivity in immune cells where even a single cognate ligand is able to activate the immune cell in the presence of large amount of noncognate ligands (Yuri Sykulev, 1996)**,** our work is distinct in that cells can change their behavior based on purely mechanical differences. Both strong and weak TGTs present the chemically identical ligands to the cells with the only difference being the mechanical stability of the tethers.

What might be the underlying mechanisms for the remarkable sensitivity to the presence of a minute number of mechanically strong ligands? We previously presented evidence that the tension threshold for cell adhesion can be reduced by lowering the membrane tension (Wang and Ha, 2013). Therefore, processes that modulate the dynamics of the cell membrane and the actin cytoskeleton linked to the membrane may be important in the observed ultra-sensitivity to strong forces. There is evidence that cell adhesion is aided by transient contacts and force generation induced by membrane undulations (Pierres et al., 2009). In addition, sugar-protein coating called glycocalyx on cell membranes may exert steric repulsion force between the cell and the ECM and may thus influence cell adhesion (Bruinsma et al., 2000;

Paszek et al., 2014; Sackmann and Smith, 2014). Therefore, we offer one possible explanation for our observation as follows. Once a cell establishes a link to a ligand on strong TGT, this stable link would lower the membrane in the surrounding area, dampening membrane fluctuations and expelling glycocalyx which normally separates the membrane from the ECM. Glycocalyx expulsion would then lead to the recruitment of more integrins to form integrin clusters (Paszek et al., 2014), making nearby ligands on weak TGTs more accessible to integrins. The dampening of membrane fluctuations and associated forces would prevent the rupture of weak tethers and the area of close contact initiated by a single strong TGT may then expand. In other words, a very small number of strong TGTs may form individual nuclei, ultimately leading to cell adhesion. In addition, the integrins recruited around the strong TGTs may become activated to obtain much higher affinity to the ligands (Wegener et al., 2007). If there are only weak tethers, membrane fluctuations would rupture weak TGTs so that stable adhesion cannot be nucleated. If there are only a few strong tethers, the initial stable contact cannot expand and cells cannot adhere.

We have also observed ultra-sensitivity from melanoma cells (B16-F1) in addition to CHO cells, but several other cell types we tested did not show this property. Future studies employing other cell types and biological

perturbation tools may be able to reveal the underlying mechanisms that set certain cells apart in terms of their ultra-sensitivity to single molecular forces. Regardless of the detailed mechanisms, our present data are consistent with the following time courses of single integrin-ligand bonds that form during initial cell adhesion. When a single integrin-ligand bond forms, the cell gradually increases the force across the bond to about 40 pN so that weak TGTs rupture. When the force reaches ~ 40 pN for just a few integrins bound through strong TGTs, the cell apparently makes a decision that the surface is rigid enough for adhesion and the force across the strong TGTs drop to a low value. Subsequent bonds only experience this low steady state force so that the weak TGTs do not rupture anymore (Fig 1.7). In this model, rigidity sensing of the underlying surface (Chan and Odde, 2008; Du et al., 2011; Elosegui-Artola et al., 2014a; Engler et al., 2006; Ghassemi et al., 2012; McBeath et al., 2004; Plotnikov et al., 2012; Schwartz, 2010; Trappmann et al., 2012; Wen et al., 2014; Yu et al., 2011b; Yu et al., 2013b) can be completed by just a few integrin-ligand bonds, raising an interesting question how the cell achieves such mechanical ultrasensitivity without amplifying noise. Future studies utilizing live cell imaging with high space and time resolution and high sensitivity may be able to test various aspects of this model.

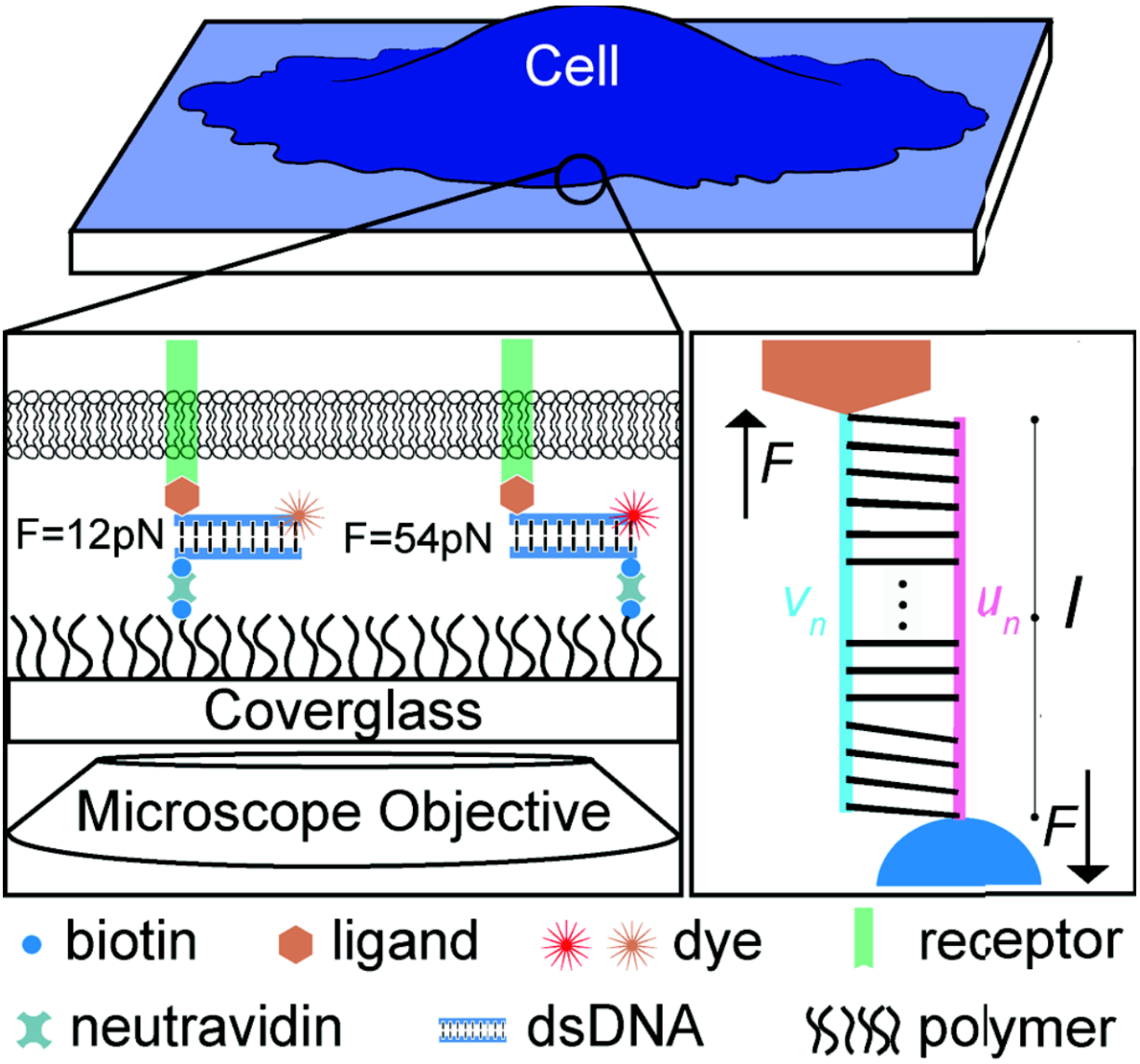
Cell
F=12pN
F=54pN
Coverglass
Microscope Objective
F
v_n
u_n
l
F
biotin
ligand
dye
receptor
neutravidin
dsDNA
polymer

Figure 1. 1

Figure 1. 1: Schematic of multiplex TGT experiment. Cells cultured are presented with two types of tension gauge tethers (TGT) simultaneously. TGTs are conjugated with the tri-peptide RGDfK which binds to integrin receptors expressed on the cell surface. Each type of TGT is also labelled with a distinct fluorophore, on the top strand, and anchored to the surface through a biotin – neutravidin linkage. Inset shows the DNA tether under tension of magnitude F applied across l base pairs in shear force configuration.

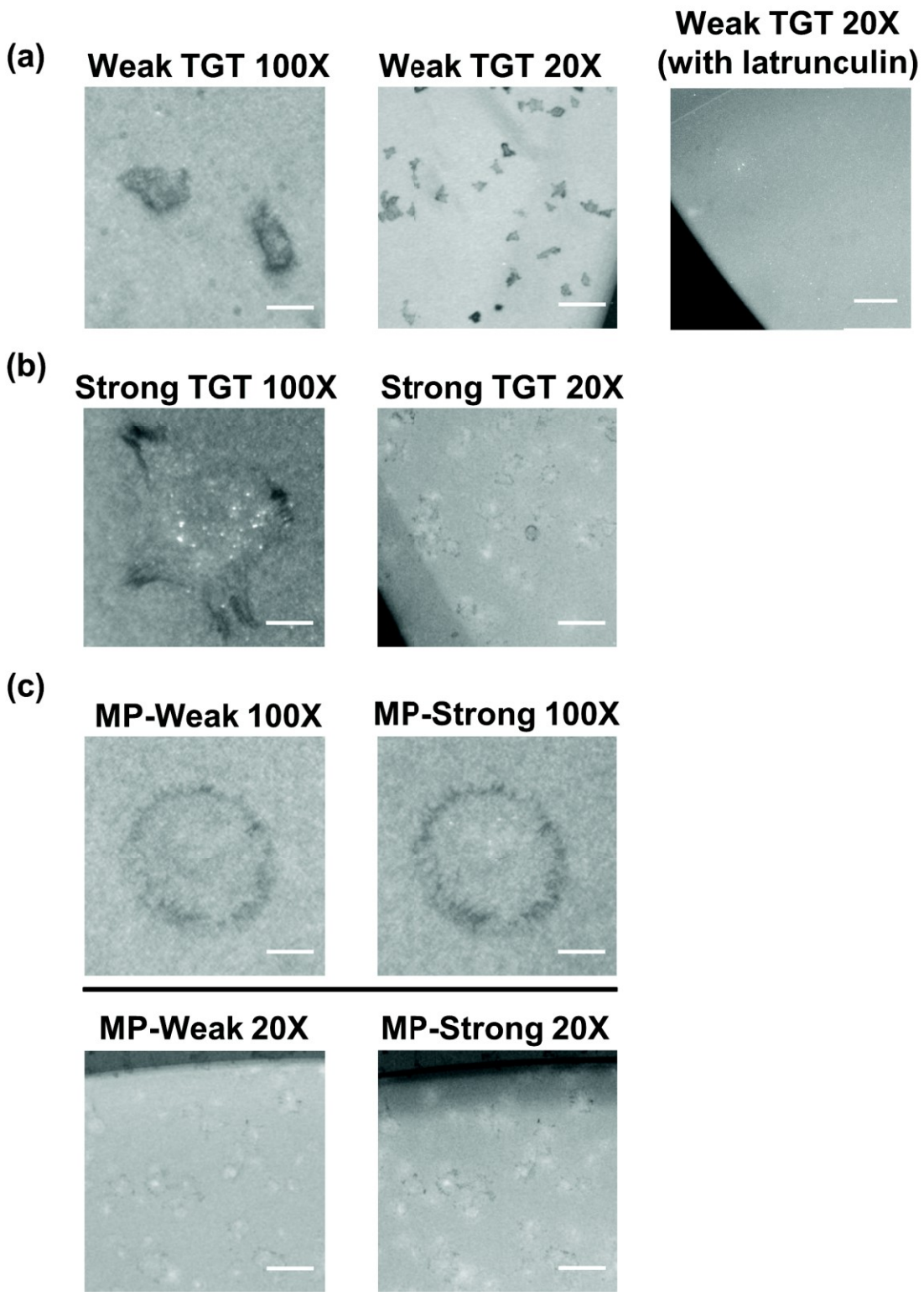
(a)
Weak TGT 100X
Weak TGT 20X
Weak TGT 20X
(with latrunculin)
(b)
Strong TGT 100X
Strong TGT 20X
(c)
MP-Weak 100X
MP-Strong 100X
MP-Weak 20X
MP-Strong 20X

Figure 1. 2

Figure 1. 2: Fluorescence images of TGT rupture with and without multiplexing. (a) Fluorescent images on the weak TGT-coated surface in 20X and 100X magnifications show uniformly dark patches beneath the cell (uniform rupture). However, when we inhibited actin polymerization by adding 1μM latrunculin A to the cell culture medium, cells did not show rupture footprint. (b) Fluorescent images on the strong TGT-coated surface show fluorescence loss mostly at the periphery of the cell (edge rupture). Bright spots are probably the vesicles containing upper strand of ruptured TGT that have undergone endocytosis. (c) Fluorescence loss patterns of weak and strong TGTs are similar and show 'edge rupture' on the multiplex TGT surface. Scale bars are 50 μm for 20X and 10 μm for 100X.

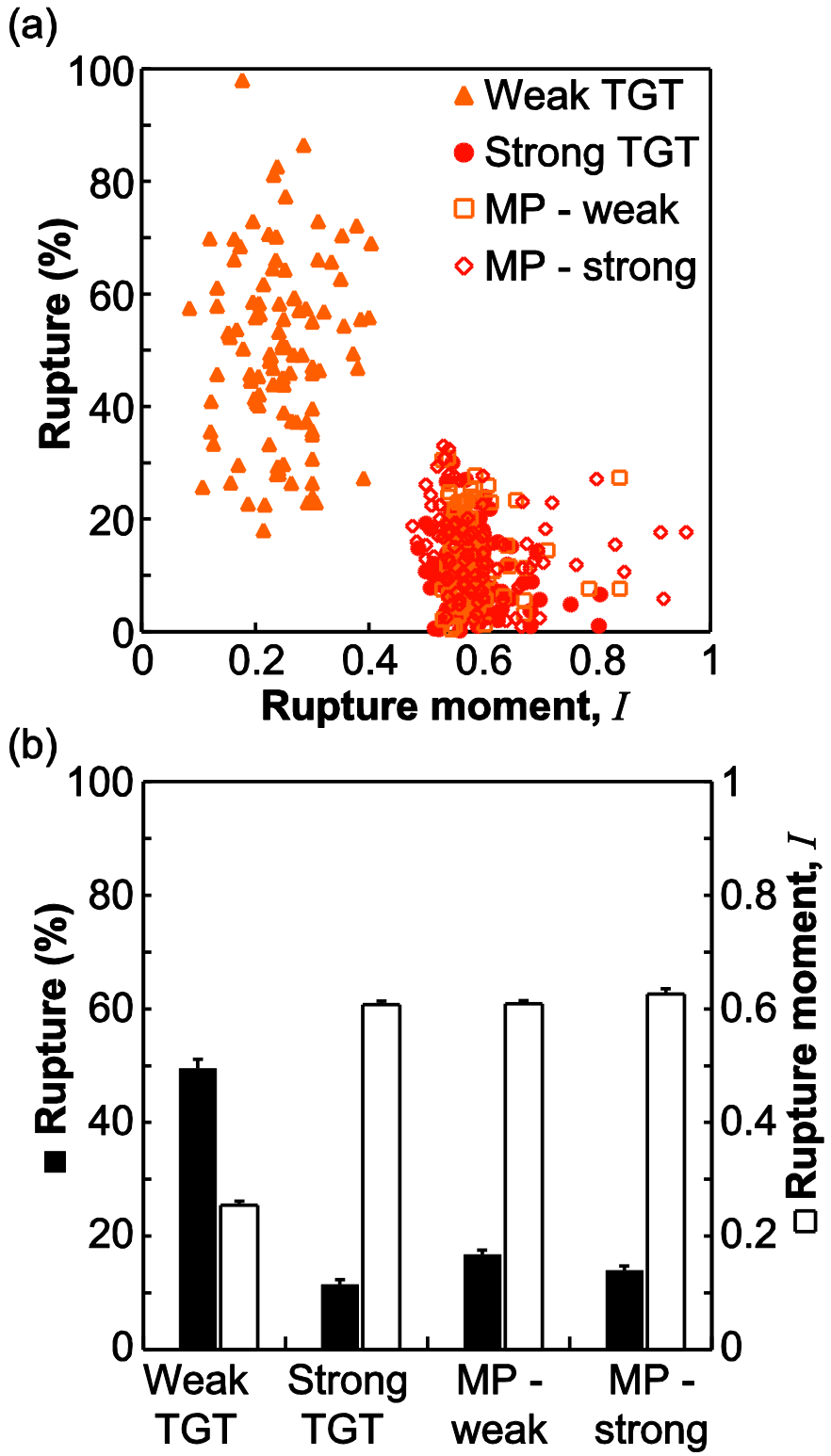
(a)
Weak TGT
Strong TGT
MP - weak
MP - strong
Rupture (%)
Rupture moment, I
0
20
40
60
80
100
0
0.2
0.4
0.6
0.8
1
(b)
Rupture (%)
Rupture moment, I
Weak TGT
Strong TGT
MP - weak
MP - strong

Figure 1. 3

Figure 1. 3: Single cell analysis of TGT rupture pattern. (a) More than 400 cells are selected and analyzed based on two variables: percent rupture and rupture moment (*I*). Each symbol represents one single cell. Percent rupture and rupture moment for the Weak TGT-coated surface (Weak TGT) are characteristic of "uniform rupture" and are clearly different from "edge rupture" characteristics seen for the Strong TGT surface (Strong TGT), and for the weak and strong TGTs on the MP surface (MP – weak and MP – strong, respectively). (b) Average values from (a). Error bars denote standard errors of mean.

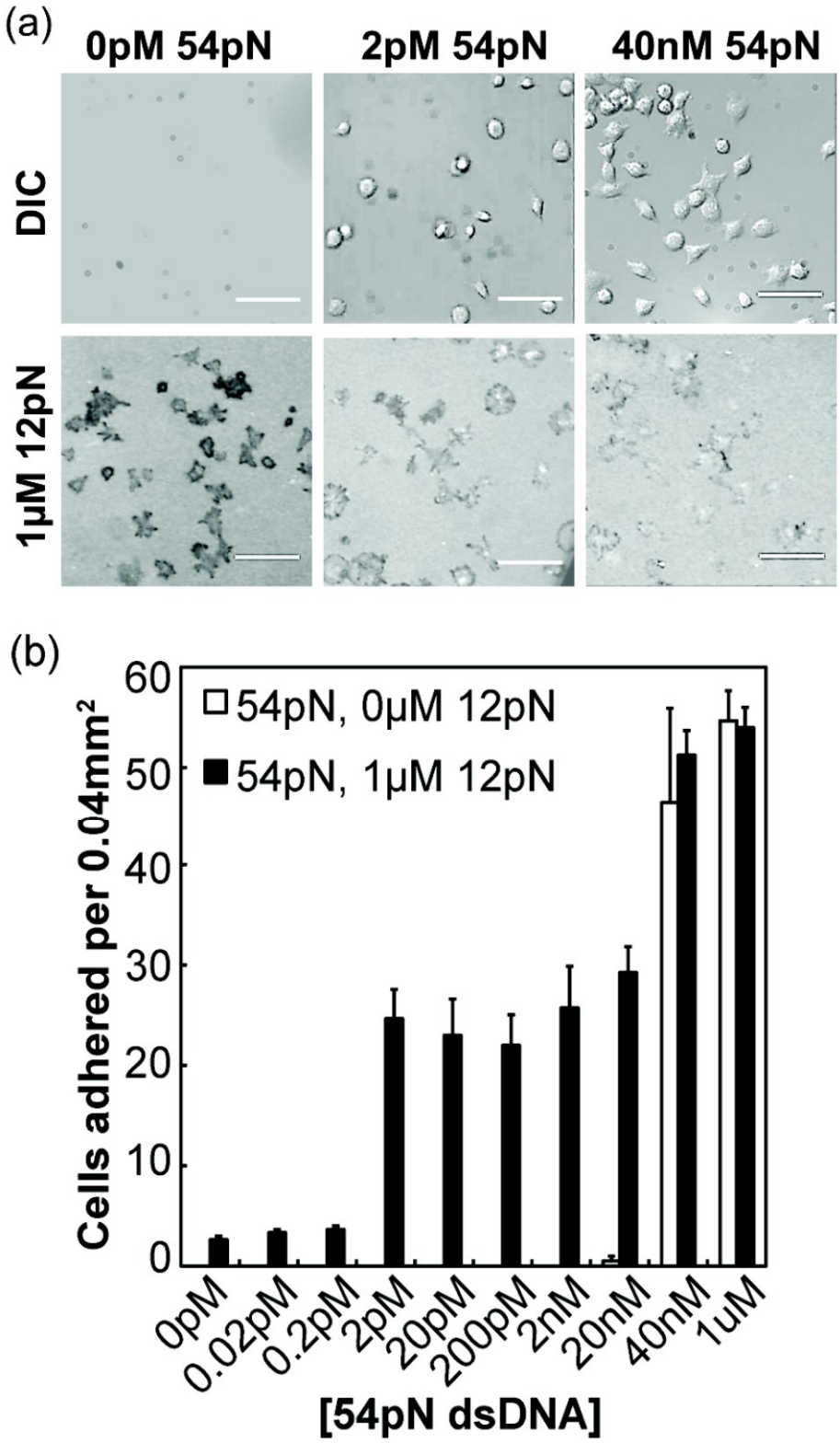
(a)
0pM 54pN
2pM 54pN
40nM 54pN
DIC
1μM 12pN
(b)
54pN, 0μM 12pN
54pN, 1μM 12pN
Cells adhered per 0.04mm²
0
10
20
30
40
50
60
0pM
0.02pM
0.2pM
2pM
20pM
200pM
2nM
20nM
40nM
1uM
[54pN dsDNA]

Figure 1. 4

Figure 1. 4: Titration of strong TGT in multiplexing experiment. (a) Representative images of cells on different MP TGT surfaces. Differential interference contrast (DIC, top) and fluorescence loss of the weak TGT (bottom). Scale bars are 50 μm. (b) Average density of adherent cells versus strong TGT incubation concentration. Only background levels of adhered cells are observed for concentrations lower than 40 nM of strong TGTs alone. However, when weak tethers are present, cells adhered for strong TGT concentration down to 2 pM but not at 0.2 pN. The cell density, although well above background levels, decreased for pM concentrations of the strong TGT. Error bars denote standard errors of mean.

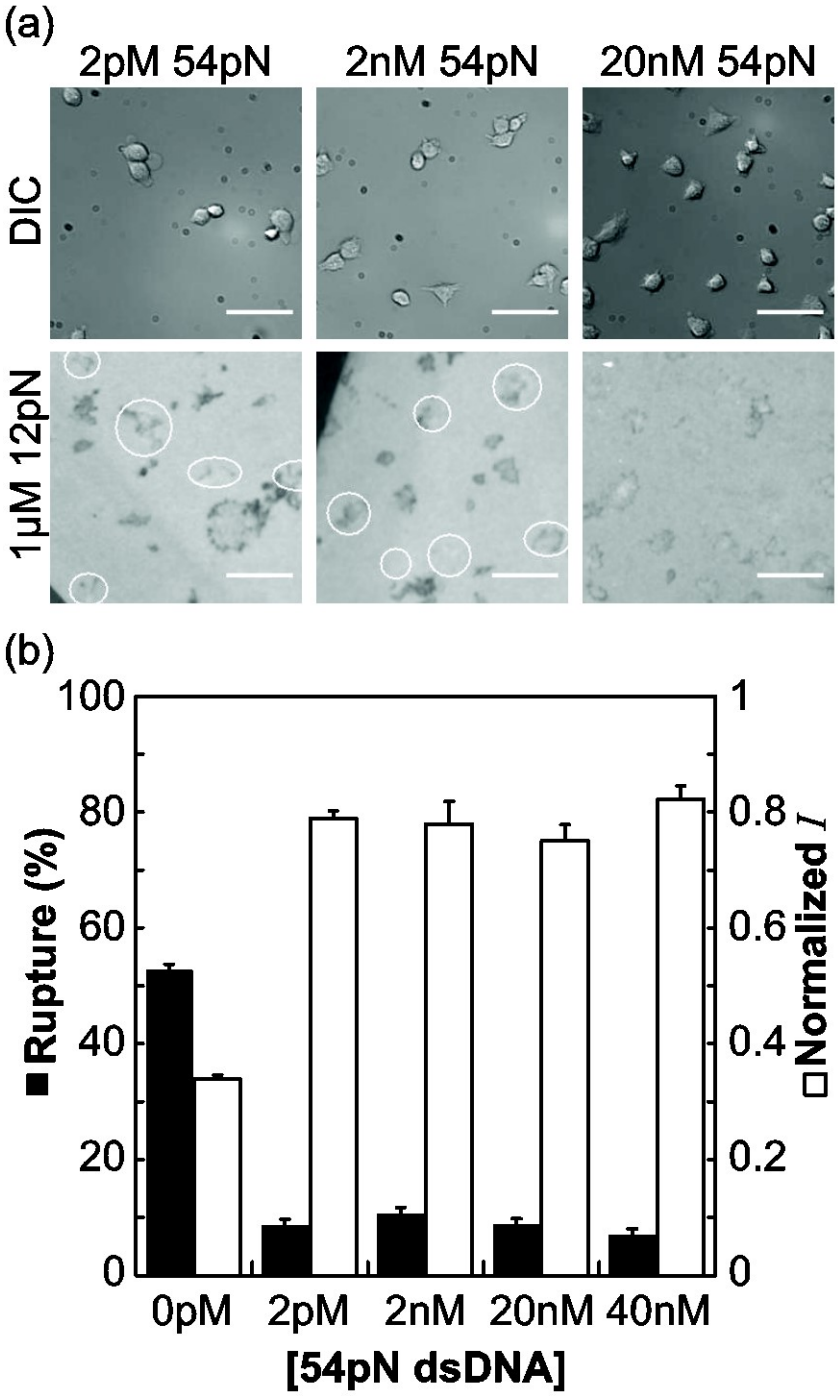
(a)
2pM 54pN
2nM 54pN
20nM 54pN
DIC
1μM 12pN
(b)
100
80
60
40
20
0
1
0.8
0.6
0.4
0.2
0
■Rupture (%)
□Normalized I
0pM
2pM
2nM
20nM
40nM
[54pN dsDNA]

Figure 1. 5

Figure 1. 5: Weak tether transformation vs. strong TGT concentration. (a) Representative images of MP TGT surfaces. DIC (top) and fluorescence loss of the weak TGT (bottom). The white outlined regions in the bottom images correspond to adhered cells in the top images. Scale bars are 50 μm. (b) Percent rupture and normalized rupture moment (*I*) are measured and averaged for cells vs strong TGT concentration. Error bars denote standard errors of mean.

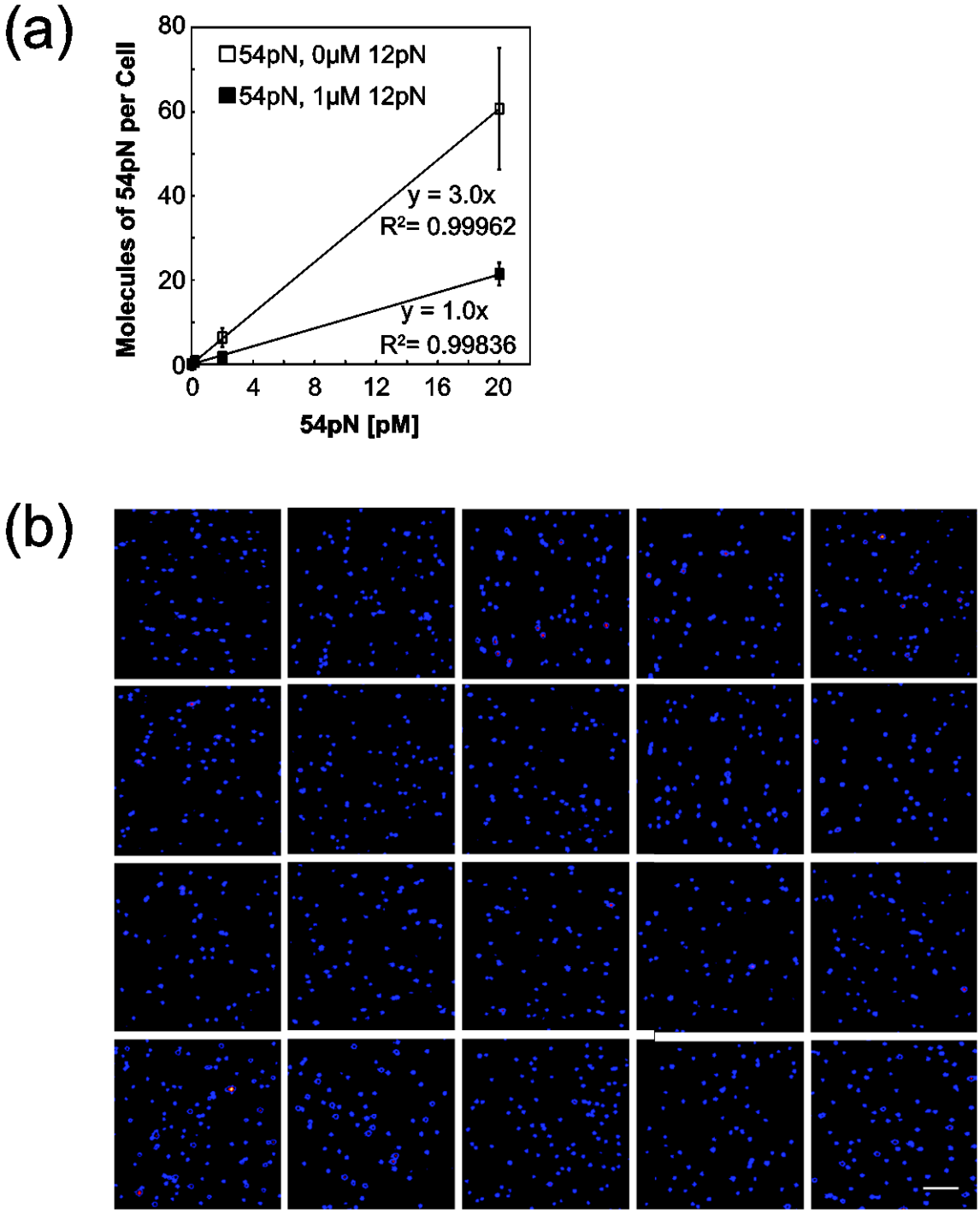
(a)
Molecules of 54pN per Cell
54pN [pM]
54pN, 0μM 12pN
54pN, 1μM 12pN
y = 3.0x
R²= 0.99962
y = 1.0x
R²= 0.99836
0
20
40
60
80
0
4
8
12
16
20
(b)

Figure 1. 6

Figure 1. 6: Single molecule measurements of strong TGT density. (a) At picomolar incubation concentrations, the average surface densities of strong TGT in the presence of unlabeled 1 μM of weak TGT were directly determined using single molecule total internal reflection fluorescence microscopy. From these measurements, the number of strong TGT per cell as a function of the pM incubation concentrations was estimated. Note that the surface density of strong tethers is three times lower when they are presented together with weak tethers, probably because weak and strong tethers can compete with each other for a finite number of binding sites on the surface. (b) 20 single molecule images of DNA tethers (50 pM Cy5-labeled strong TGTs & 1 μM unlabeled weak TGTs during incubation) show that there is no nonrandom clustering of tethers. Scale bar in the lower right image is 5 μm.

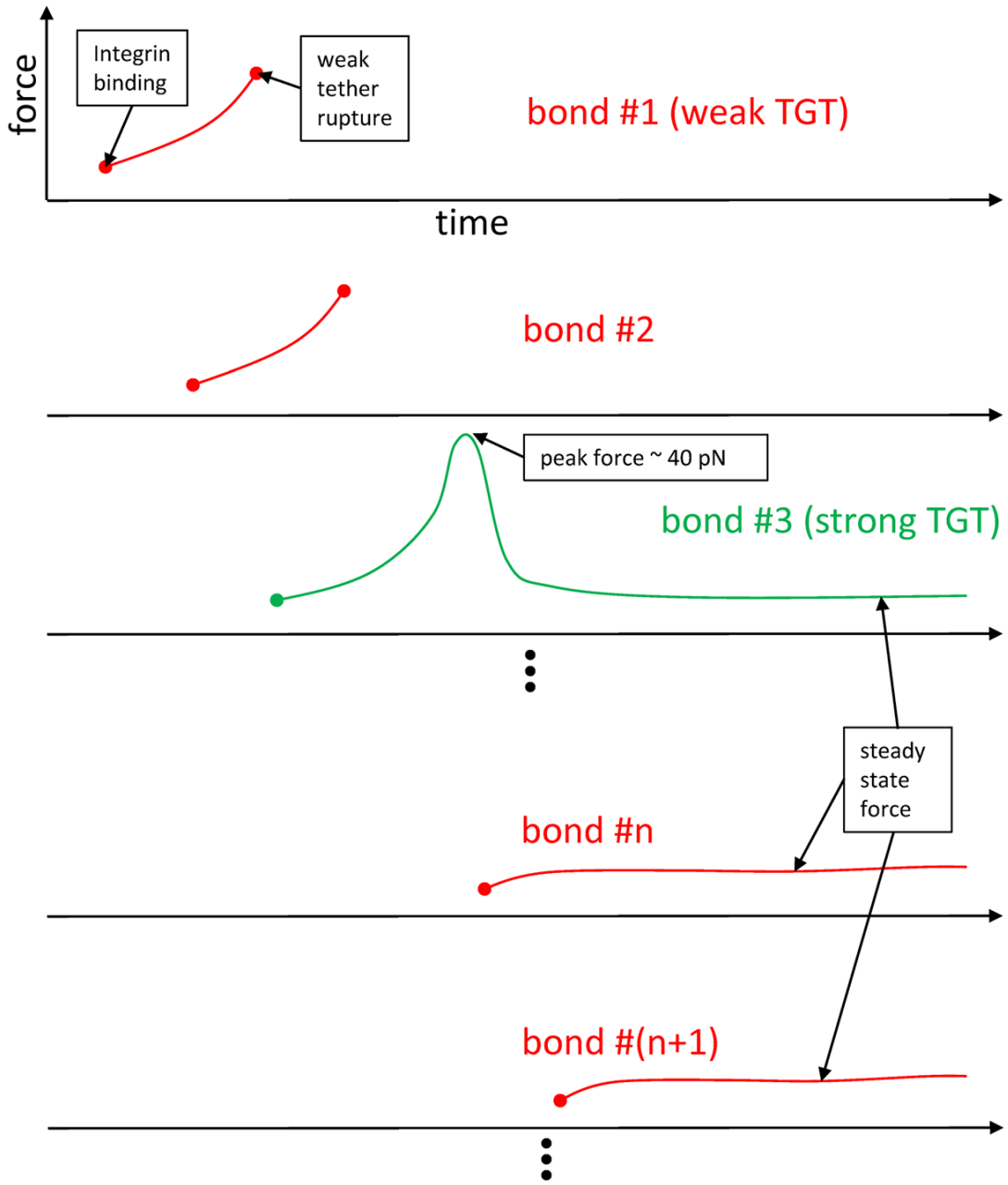
force
Integrin binding
weak tether rupture
bond #1 (weak TGT)
time
bond #2
peak force ~ 40 pN
bond #3 (strong TGT)
steady state force
bond #n
bond #(n+1)

Figure 1. 7

Figure 1. 7: Proposed time courses of mechanical engagements through single integrin-ligand bonds. A cell grabs a ligand attached to the surface through a weak tether and applies gradually increasing force until the weak tether ruptures. If a strong tether is pulled, the 40 pN threshold force for adhesion is reached, telling the cell that the substrate is rigid enough for adhesion. Then, the force through the bond drops to a low, steady state value, and subsequent bonds experience only this lower force. The cell no longer needs to apply strong forces because it has already determined that the substrate is rigid enough.

Chapter 2

Ultra-sensitivity of Cell Adhesion to the Differential Mechanical Cues and Requirement of Reversibility

INTRODUCTION

The extracellular matrix (ECM) presents physical cues that cells continually probe. These physical messages have crucial roles in regulating diverse cellular physiologic or pathologic processes(Bonnans et al., 2014; Discher et al., 2005; Elosegui-Artola et al., 2014b; Kumar and Weaver, 2009; Liu et al., 2015; Wozniak and Chen, 2009). The transmembrane receptor protein called integrin interacts with the ECM to transmit information about the surrounding to inside the cell via the interaction with membrane-associated macromolecular protein assemblies called focal adhesions (FAs) and the regulation of the 3D actin cytoskeleton lattices (del Rio et al., 2009; Engler et al., 2006; Friedland et al., 2009; Gordon et al., 2015; Grashoff et al., 2010; Hoffman et al., 2011; Ingber, 2006; Koo et al., 2002; Morimatsu et al., 2013; Oakes and Gardel, 2014; Sawada et al., 2006; Stabley et al., 2012; Wang et al., 2005; Watt and Huck, 2013). The ECM itself is a diverse interaction platform and is heavily investigated for fundamental cellular processes and functions (Chiquet et al., 2009; Dobereiner et al., 2004; Evans and Calderwood, 2007; Geiger et al., 2009; Geiger and Yamada, 2011; Grashoff et al., 2010; Halder et al., 2012; Jurchenko et al., 2014; Liu et al., 2013; Morimatsu et al., 2015; Zhang et al., 2014). Cell interaction with such a mechanically heterogeneous ECM activates downstream intracellular

signaling to dictate critical cellular functions including cell adhesion, migration, proliferation, or apoptosis. Therefore, it is important to understand force dependent fundamental cellular processes like cell adhesion and spreading in heterogeneous environments.

Previously, many studies attempted to understand cell adhesion and spreading behavior modulated by average molecular forces across integrins(Yu et al., 2011a; Yu et al., 2013a). Earlier studies using fibronectin as a substrate investigated early cell adhesion and spreading and modeled distinct phases of cell adhesion(Dubin-Thaler et al., 2004; Dubin-Thaler et al., 2008; Giannone et al., 2004). These findings, although useful observations, are short of underlying understanding for molecular mechanism of early cell adhesion events primarily due to lack of precise control of mechanical cues. Many other studies investigated Rho-GTPases(Hall, 1998; Nobes and Hall, 1995), tyrosine kinases(Mitra and Schlaepfer, 2006), structural cytoskeletal units and associated contractile elements(Chan and Odde, 2008; Schwartz, 2010) during cell adhesion and subsequent modulation of cellular behavior. The mentioned studies however involve further downstream activities and do not capture early events in cell adhesion. They also depended on the bulk properties of the underlying substrate stiffness, which inherently lacks precise control at the molecular level.

In order to study involvement of single molecular forces in cellular processes, we developed tension gauge tether (TGT) technique (Wang and Ha, 2013) and by utilizing this technique we demonstrated that single molecular forces at the cell-substrate interface determines whether cells can adhere to the surface (Wang and Ha, 2013) and control the degree of cell spreading (Chowdhury et al., 2015). In the current work, we utilized short (18 base pairs) double-stranded DNA with a defined range of rupture forces to limit molecular forces across single integrins. One strand of the DNA is conjugated to a ligand for specific integrin binding and the other strand is immobilized to the surface via neutravidin-biotin interactions. An array of tethers with defined tension tolerances is constructed by changing the biotin position on the DNA strand. When the ligand and biotin are placed on the same end of the DNA, TGTs sense an unzipping loading configuration upon applying force thereby providing a weak tension tolerance of 12 pN. When the ligand and biotin are placed on the opposite ends, TGTs experience a shear-loading configuration thus providing a stronger tension tolerance of 54 pN. TGTs with intermediate rupture forces were also constructed by positioning the biotin at locations intermediate between the two extremes.

Using the TGT technique we previously showed that cells exert about 40 pN of peak forces during initial cell adhesion. Therefore, weaker TGTs

with tension tolerance less than 43 pN, namely 12 pN, 23 pN and 33 pN did not support cell adhesion. In more physiological settings, we can anticipate that the mechanical cues would be heterogeneous. In a recent study where we mixed strong and weak TGTs to better mimic native cellular environments, we demonstrated that just a few copies of strong (~ 54 pN) TGTs per cell are enough for cell adhesion and spreading as long as there is a high density of weak tethers which implies ultrasensitivity of cells to strong ligands (Roein-Peikar et al., 2016). In the present study, we further investigated the effect of mechanically heterogeneous environment during early stages of cell adhesion.

RESULTS AND DISCUSSION

Cell adhesion is supported on a multiplexed weak TGT surface

To create a mechanically heterogeneous surface, we multiplexed two weak tethers, namely 12 pN and 23 pN TGTs, neither of which supports cell adhesion if presented individually on a mechanically homogenous surface. Cy3 and Cy5 fluorophores were conjugated to the 5' end of upper strand of 12 pN and 23 pN TGT, respectively, to independently monitor the rupture pattern of these weak TGTs. A ligand called cyclic-RGDfK, specific for $\alpha_v\beta_3$ integrins (Aumailley et al., 1991; Gurrath et al., 1992; Pfaff et al., 1994), was also conjugated on the 3' end of the upper strand.

We prepared three different TGT-surfaces by incubating PEG-passivated and neutravidin-coated glass coverslip with 1 μM 12 pN TGT (12 pN-only surface), 1 μM 23 pN TGT (23 pN-only) or a mixture of 0.5 μM 12 pN TGT and 0.5 μM 23 pN TGT (12 pN & 23 pN) (Fig. 1). Equal number of Chinese hamster ovary (CHO) cells were plated on the three surfaces for half an hour in 37° C and were washed gently before imaging. As reported before(Wang and Ha, 2013), very few cells adhered to the12 pN-only and 23 pN-only surfaces (Fig. 2a) with dark patches in fluorescence images due to >60 % rupture of TGTs caused by cells that were rinsed off (Fig. 2c). Surprisingly, a high number of cells adhered on the 12 pN & 23 pN surface with about 10% TGT rupture underneath (Figs. 2b, c). Therefore, mixing the two weak TGTs allow cell adhesion even though individually neither of the two is strong enough to support cell adhesion. Moreover, cells left behind two distinct types of footprints. In the case of 12 pN-only or 23 pN-only surfaces, cells uniformly ruptured the weak TGTs underneath the cells (Fig. 2a). In contrast, we observed an edge rupture pattern (mostly at the cell periphery) for both TGTs on the 12 pN & 23 pN surface (Fig. 2a). Therefore, the presence of both weak tethers of different tension tolerance somehow induces the cell to make a decision to adhere and to no longer apply strong forces that can rupture these weak TGTs (Roein-Peikar et al.). The edge rupture pattern is

caused by myosin-dependent forces at focal adhesions that develop after cell adhesion and spreading (Wang et al., 2015).

We next performed similar experiments by pairwise mixing the following TGTs: 12 pN, 23 pN, 33 pN, 43 pN and 54 pN (0.5 μM of one TGT mixed with 0.5 μM of another). All pairwise combinations allowed cells to adhere even in the cases of both TGTs weaker than 40 pN (12 pN & 33 pN, 23 pN & 33 pN, and 12 pN & 23 pN) (Fig. 3). Therefore, cells seem to be performing differential force measurements during cell adhesion decision making.

Ultrasensitivity of cells to single molecules

We next tested how much 23 pN TGT is needed to enable cell adhesion through differential force sensing when they are presented together with a high density of 12 pN TGT by progressively lowering the concentrations of relatively stronger tethers and found that 1 pM of 23 pN TGT mixed with 1 μM of 12 pN TGT during TGT incubation. Single molecule fluorescence imaging of Cy3-labeled 23 pN TGT mixed with unlabeled 12 pN TGT allowed us to calibrate the average surface density of 23 pN TGT, and we could estimate that on average about two 23 pN TGTs are under adherent cells at 1 pM incubation concentration, assuming the average area of 600 μm^2 for adherent cells (Chowdhury et al., 2015). Thus, cell adhesion is ultrasensitive

to a very small number of mechanically strong ligands. This is reminiscent of our previous observation that on average about two RGDfK ligands presented through 54 pN TGTs are enough to support cell adhesion if there is a high density of 12 pN TGTs present as well. This corresponds to ultrasensitivity of cells to single molecules of relatively stronger TGTs per cell which we call The Princess and the Pea effect (PnP) and refers to the popular fairy tale (Fig. 4a). This implies that cells are ultra-sensitive to the presence of very few relatively stronger –but still weak to secure the cells by themselves- tethers. This observation is similar to our earlier study where 1 pico molar (1 pM) of a strong TGT such as 54 TGT multiplexed with 1 micro molar (1 μM) of 12 pN TGT is sufficient to support cell adhesion (Roein-Peikar et al., 2016).

We expanded our investigation to study the PnP with other combinations of weak and relatively strong tethers. Based on these studies, we constructed a two dimensional table with horizontal axis representing 1 μM of different tethers and vertical axis with 1 pM of various tethers (Fig. 4c and 4d). The highlighted diagonal blocks in the table at Fig. 4d represent a mechanically homogeneous surface where cells adhere to the surfaces covered with TGTs with rupture force of higher than 40pN, namely 43 pN and 54 pN, which is in agreement with our previous report(Wang and Ha, 2013). The outlined red box in the lower left corner shows the top three off-diagonal

blocks exhibit PnP while the bottom three off-diagonal blocks do not. It is clear that the lower concentration tethers need to be stronger than high concentration tethers to exhibit UCE.

Other than CHO-K1 cells, we observed adhesion of mouse skin melanoma cell called B16-F1 (supplementary Fig. 1) and also a glycosylation defective CHO-K1 cell type called Lec-8 (data not shown) to 12 pN & 23 pN and PnP surface but not to 12 pN-Only or 23 pN-Only surfaces.

Similarity between 54 pN, 12 pN & 23 pN and PnP surfaces

Comparing the edge rupture pattern between the surfaces covered with strong TGT -with a rupture force of 54 pN, 12 pN & 23 pN surface and PnP surface showed the degree of rupture to be similar (Supplementary Fig. 2).

Inhibiting the Focal Adhesion Kinase (FAK) by adding 100 μM FAK inhibitor PF573-228 to the cell culture medium during incubation in 37℃ did not interrupt the cell adhesion and did not change the rupture pattern on the 12 pN & 23 pN and PnP surface. Similarly, cells on the 54 pN-Only surface did not show any change in cell adhesion or fluorescent footprint pattern with the inhibition of FAK. Inhibition of FAK was confirmed by utilizing a fluorescence resonance energy transfer (FRET) based FAK biosensor (Seong et al., 2011) (Fig. 2b, c and Supplementary Fig. 3). This implies that early adhesion of the cells to the multiplexed surface is not dependent on FAK

activation or anything downstream of FAK. The only entity that is upstream of FAK is integrin, which makes it the candidate for having the major role in our observed phenomenon. Additionally, the cells on 54-Only surface showed the same FAK activity as 12 pN & 23 pN and PnP surface in the control experiment without adding FAK inhibitor (Supplementary Fig. 3b).

Furthermore, inhibiting myosin II by adding 10 μM or 50 μM blebbistatin to the cell culture medium did not prevent adhesion of the cells to the 12 pN & 23 pN and PnP surface either. With blebbistatin treatment, however, we observed even lower rupture characteristics. The lack of rupture of TGTs at the periphery of the cells suggests that myosin II is the determinant of the rupture of TGTs at the periphery of the cells (edge rupture fluorescent footprint pattern), while cell adhesion itself is not necessarily dependent on myosin II (Fig. 2b, c, Supplementary Fig. 4).

Moreover, we compared focal adhesion (FA) forming capabilities of cells on multiplexed 54 pN, 12 pN & 23 pN and PnP surfaces. We did not observe any significant difference in FA formation on these surfaces (Supplementary Fig. 8). This is consistent with the result we got from the FAK activity test using the fluorescence resonance energy transfer (FRET) based FAK biosensor, in which we observed the FAK activity is similar in cells

adhered to 54 pN surface, 12 pN & 23 pN surface and PnP surface (Supplementary Fig. 3).

23 pN TGTs form supporting membrane holders to endorse cell adhesion

We reported in our earlier work that tension threshold for cell adhesion can be reduced by lowering the membrane tension thereby suggesting membrane dynamics play a critical role in the process(Wang and Ha, 2013). This is in agreement with other reports suggesting force fluctuations mediated by membrane undulations affect cell adhesion(Pierres et al., 2009; Sackmann and Smith, 2014). Since our present data also pointed at integrins to be responsible for this distinct characteristic of cell adhesion, we focused on integrins and associated membrane dynamics.

We designed two different sequences of 12 pN (Seq1) and 23 pN (Seq2) TGTs as indicated in Fig. 5a (please see Methods section for making TGT). Both of these sequences had the same ratio of different nucleotides and were both checked for the minimum possibility of making hairpins, hetero-dimers or self-dimers. Adding 1 μM sequence 1 ssDNA (upper-Seq1, green) into the cell culture medium while the cells were incubated in 37°C inhibited cells from adhering to the multiplexed surface (Fig. 5a, 2nd row). The presence of upper-Seq1 (green) ssDNA causes very few cells to adhere to the surface and

fluorescent footprint of detached cells is uniform rupture (Fig. 5b, c). Adding the lower-Seq1 ssDNA (blue) had similar effect of cells not adhering to the multiplexed surface (Supplementary Fig. 6). However, adding 1 μM sequence 2 ssDNA (upper-Seq2, black) did not prevent the cells from adhering to the multiplexed surface and high cell density with edge rupture fluorescent footprint of TGTs was observed in this case (Fig. 5a, 3rd row and Fig. 5b, c). Similarly, adding lower-Seq2 ssDNA (red) to the medium also allowed cells to adhere to the multiplexed surface (Supplementary Fig. 6). Adding unrelated ssDNA to the medium did not affect cell adhesion to the multiplexed surface negatively.

Likewise, adding free ssDNA associated to the upper or lower strand of weaker tether in all three upper off-diagonal PnP surfaces in Fig. 5 prevented them from cell adhesion while adding free ssDNA associated to the upper or lower strand of relatively stronger tether did not affect the cell adhesion in those three upper off-diagonal conditions.

Single molecule total internal reflection fluorescence microscope (TIRF) experiment was performed with ssDNA added to the medium during incubation in order to check the possibility that the upper strand of TGT could be substituted by the free competitor ssDNA in the medium. Substitution within the half hour of incubation was not observed (Supplementary Fig. 7).

These results suggest that the relatively stronger TGT of the two weak TGTs, i.e., 23 pN TGT acts as a supporting tether allowing the membrane to stay close to the surface, which results in damping the membrane undulations and thereby preventing or decreasing force application to the weak tethers. This eventually leads to the prevention of rupture in the weaker TGT, i.e. 12 pN TGT. Even if the 12 pN TGTs are opened, 23 pN TGT acting as a supporting membrane holder aids 12 pN TGTs to undergo re-annealing by keeping the cell membrane close to the surface. Hence, the mechanically heterogeneous surface supports cell adhesion although both type of TGTs do not support cell adhesion by themselves (See the schematic in Fig. 6).

DISCUSSION

One surprising result we got was that cells adhere to the multiplexed 12 pN & 23 pN surface while they do not adhere to a surface with 12 pN-Only or 23 pN-Only surface. On the 12 pN & 23 pN surface the probability that weaker TGTs (12 pN TGT) get ruptured due to the undulations of cell membrane is higher than that of 23 pN TGTs. In this situation, relatively stronger TGTs (23 pN TGT) make membrane holders for the weak tethers (12 pN TGTs) that exist around them. The rupture of 12 pN TGT is reversed and ruptured 12 pN TGT is re-annealed due to the membrane holder, i.e. 23 pN TGT, which holds the membrane closer to the surface like a tent peg. This

happens by keeping the upper ssDNA of 12 pN TGT that are attached to the integrin, close to the ruptured lower ssDNA that is anchored to the surface. Similar to the 12 pN & 23 pN surface, on the PnP surface the reversibility and re-annealing of weaker tethers due to the support from relatively stronger supporting membrane holders, i.e. 23 pN TGT, results in keeping the cells adhered to the surface. Therefore, the cells appear to be able to perform relative force measurements instead of absolute force measurements.

The surprising difference between 12 pN & 23 pN and PnP is that just few relatively stronger tethers can keep the cells adhered which implies the ultra-sensitivity of cells. All the upper off-diagonal conditions in Fig. 5b or 5c that show cell adhesion consist of the surfaces with high concentration of weaker TGT multiplexed with lower concentration of relatively stronger TGT. The lower off-diagonal conditions in which a few relatively weaker TGTs are multiplexed with many stronger TGTs, cannot withstand cell adhesion. The reason for the detachment of the cells is that those conditions lack a few membrane holders that are stronger TGTs compared to the majority of TGTs on the surface. In other words, absolute value of rupture force for TGTs is not the determinant of cell adhesion for weak tethers. The critical factor for cell adhesion is to have the relatively stronger supporting membrane holder next to them even if the relatively stronger TGTs do not support cell

adhesion on their own or even if their number would be at a low level of 2 single molecules per cell.

A single molecule of relatively stronger TGT, as the tent peg, keeps an area of the cell membrane around it close to the surface which causes the reversibility of rupture for the relatively weak tethers around it. Based on our data even one single molecule of stronger tether can make the entire cell committed to adhesion to the surface (Fig. 6b). In case of two molecules, there will be a strip of area between the stronger TGTs or tent pegs in which the cell membrane stays closer to the surface and causes the reversibility of weaker tethers. If there are three molecules with the role of tent pegs, either three strips of area on the cell membrane will be formed that connect those three tent pegs and stay close to the surface or a triangle will be formed. Based on our last study the cells decide on adhesion to the surface over the first 5 minutes of landing and they will not pull a high force at the level of 40 pN on the TGTs after deciding on commitment to adhere (Roein-Peikar et al., 2016; Wang and Ha, 2013). In the current study the presence of single molecules of relatively stronger TGT makes the cells committed to adhere and they do not apply high force afterwards which leads to staying attached to the surface.

Adding the ssDNA complementary to either strand of the weaker TGT results in detachment of the cells and is a confirmation for the hypothesis of

reversibility of weak tethers in adhesion to 12 pN & 23 pN surface or PnP surface. Rupture of weaker TGT in 12 pN & 23 pN or PnP surface while there is no ssDNA is reversible due to the supporting membrane holder that keeps the membrane closer to the surface like a tent peg. However, adding a high concentration of ssDNA complementary to the weak tether disrupts the reversibility of rupture of weak tethers because they interact with the ruptured weaker tether. Additionally, lack of cell detachment by adding the ssDNA associated to the stronger tether is due to absence of temporary rupture in the relatively stronger tether which is another hint that confirms the reversibility or re-annealing of weak tether hypothesis.

METHODS

Cell Culture

CHO-K1 cell line (Catalog No. CCL-61), B16-F1 cell line (Catalog No. CRL-6323) and Lec-8 cell line (Catalog No. CRL-1737) were obtained from ATCC. CHO-K1 and Lec-8 cells were cultured in Alpha-MEM medium and B16-F1 cells were cultured in DMEM medium. Both Alpha-MEM and DMEM were containing 100 units/ mL penicillin, 100 µg/mL streptomycin, and 10% fetal bovine serum (HyClone, Logan, UT, USA). Cells were kept in a humidified atmosphere of 5% CO2 at 37°C.

Fabrication of tension gauge tether (TGT)

Complementary 18 base pair single strand DNAs (ssDNA) were used to make the TGTs (/5Cy3/GGC CCG CAG CGA CCA CCC/3ThioMC3-D/ for upper strand, /5AmMC6/ GGG TGG TCG CTG CGG GCC/3' for 12 pN lower strand and 5'/GGG /iAmMC6T/GG TCG CTG CGG GCC/3' for 23 pN lower strand). RGDfK (Peptides International) was conjugated to the thiol group on the upper strand of DNA. Upper and lower strands were annealed. We followed the protocols in our previous papers for conjugation and annealing(Chowdhury et al., 2015; Roein-Peikar et al., 2016; Wang and Ha, 2013; Wang et al., 2015a).

Preparing the surfaces

PEGilated slides were made while ratio of biotin-PEG (Bio, Inc.) to m-PEG-SVA (Bio, Inc.) was 1:22. After treating the surface with 200 μg/mL neutravidin (Thermo Scientific) for 5 minutes in room temperature, the surface was rinsed several times with T50 solution. 3μL of solution containing TGT was incubated on the surface for 10 minutes in the room temperature. The surface was rinsed with DPBS several times.

Preparation of cell solution

Cells were detached from culture flasks using a mild detaching solution, Ethylenedediaminetetraacetic acid (EDTA) solution, to preserve the integrity

of cell membrane protein. Before incubating the cells with EDTA at 37°C, they were rinsed twice with PBS buffer. The cells were incubated at 37°C for 10 minutes and dispensed by pipetting. Cells were spun down and re-suspended in Alpha-MEM medium (9144, Irvine Scientific) with a concentration of 10^6 /mL. Here are the ingredients of EDTA solution: 100mL 10X HBSS, 10mL1M HEPES (PH7.6), 10mL 7.5% sodium bicarbonate, 2.4 mL 500mM EDTA, 1L H_2O.

Incubation of the cells on the surface, fixation and imaging

After detachment of the cells they were centrifuged and re-suspended in the medium without FBS. The cells were added to the surface and incubated in 37°C for 30 minutes. Cells were gently washed and were fixed using 4% Paraformaldehyde (PFA) on ice for 10 minutes. PFA was rinsed with cold DPBS. Images were taken using Epifluorescence microscopy (Zeiss Axiovert 200M).

Image Analysis

Rupture percent was measured using this formula:

$$Rupture\ (\%) = \frac{MI_{bright} - MI_{cell}}{MI_{bright} - MI_{dark}}$$

(2)

where *MI* is the mean fluorescence intensity. Value of *MI* was measured in ImageJ (open-source software developed by the National Institutes of Health).

‘cell’ means the area underneath the cell; ‘bright’ means the nearby bright area without any attached cell and ‘dark’ means the background dark area off of the TGT spot.

For 12 pN-Only and 23 pN-Only fluorescent images, regions for analysis were selected from fluorescent images as no cells were attached on the surface. For 12 pN-Multi and 23 pN-Multi images DIC microscopy images were used to select the area and corresponding area on the fluorescent image was analyzed.

Because the image analysis of the weak TGT-Only experiments (with no adhered cells) is different from multiplexing experiments (in which the cells are adhered), a control experiment was performed to rule out any sort of impartiality. Regions were selected in two ways for the mechanical heterogeneous environment image (with adhered cells). In one, the regions were selected on the fluorescent image and in another method regions were selected from DIC images and the percent rupture was calculated on the corresponding region on the fluorescent image. Percent ruptures from the two analyses were within standard deviation of each other: 9.12%±0.89 and 9.01%±0.82 for first and second methods, respectively.

FAK activation assay

The cytosolic FAK biosensor was developed based on FRET. The biosensor was made by fusing the SH2 domain from c-Src, a flexible (GSTSGSGKPGSGEGS, and a FAK substrate peptide (ETDDYAEIIDE) between the N-terminus ECFP and the C-terminus YPet. The cells were transfected with this construct and detached after one day and kept in 1% agarose gel in culture medium for 1 h. After seeding the cells on different surfaces for half an hour, they were imaged with Zeiss Axiovert microscope and the MetaFluor 6.2 software (Universal Imaging). The fluorescent intensity of non-transfected cells was considered as the base signal and subtracted from the ECFP and YPet signals of transfected cells. The pixel-by-pixel ratio images of ECFP/YPet were calculated based on the background-subtracted fluorescence intensity images of ECFO and YPet by using the MetaFluor software.

Single Molecule Experiment

Imaging Cy5 labeled TGTs in the single molecule level was conducted by our custom built microscope setup. Olympus IX-71 inverted microscope with 100X NA 1.4 SaPo oil objective was combined with a red laser (647nm) excitation path (DL640-100-AL-O, Crystalaser and LS6T2, Unibliz). The laser was expanded by 7.5X, reflected by a dichroic mirror (Semrock

FF408/504/581/667/762-Di01-25X36) and sent to the sample with a total internal reflection angle. The emission was collected by the objective and filtered by an emission filter (Semrock FF01-594/730-25) and notch filters (Semrock NF01-568/647-25X5.0 and NF01-568U-25), and was imaged on an EMCCD camera (DV887ECS-BV, Andor Tech). A DIC image of a single cell area was taken firstly, then Cy5 labeled TGTs were imaged for the same area.

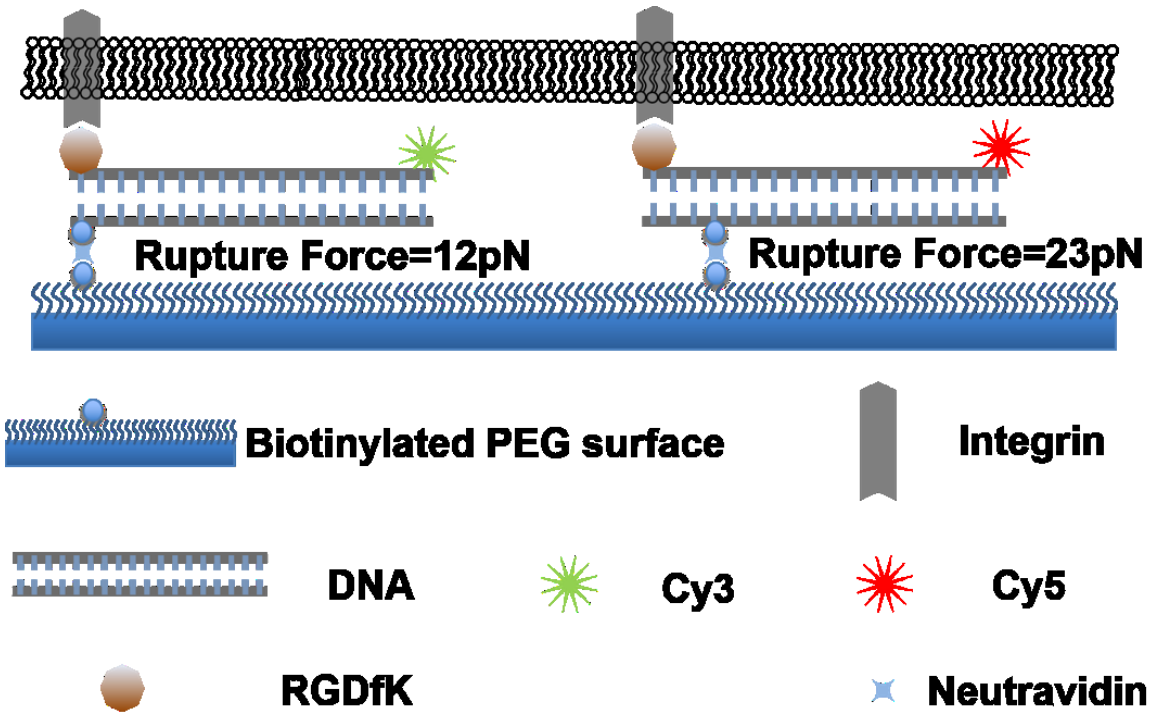
Rupture Force=12pN
Rupture Force=23pN
Biotinylated PEG surface
Integrin
DNA
Cy3
Cy5
RGDfK
Neutravidin

Figure 2. 1

Figure 2. 1: Schematic of the interface between the cell and a mechanically heterogeneous surface. Cells are adhered on a surface covered with tension gauge tethers (TGTs) with two different rupture forces (12 pN and 23 pN) that makes the surface mechanically heterogeneous. However, cells do not adhere to a surface with only 12 pN TGT or to a surface with only 23 pN TGT. 12 pN TGT has Cy3 and 23 pN TGT has Cy5 dye on the top strand of DNA. On the upper strand of TGT there is RGDfK which is the ligand for the transmembrane protein (integrin $\alpha_v\beta_3$). Note that TGTs are anchored to the surface through a biotin – neutravidin linkage and position of biotin attached to the lower strand of DNA determines the rupture force of the tether.

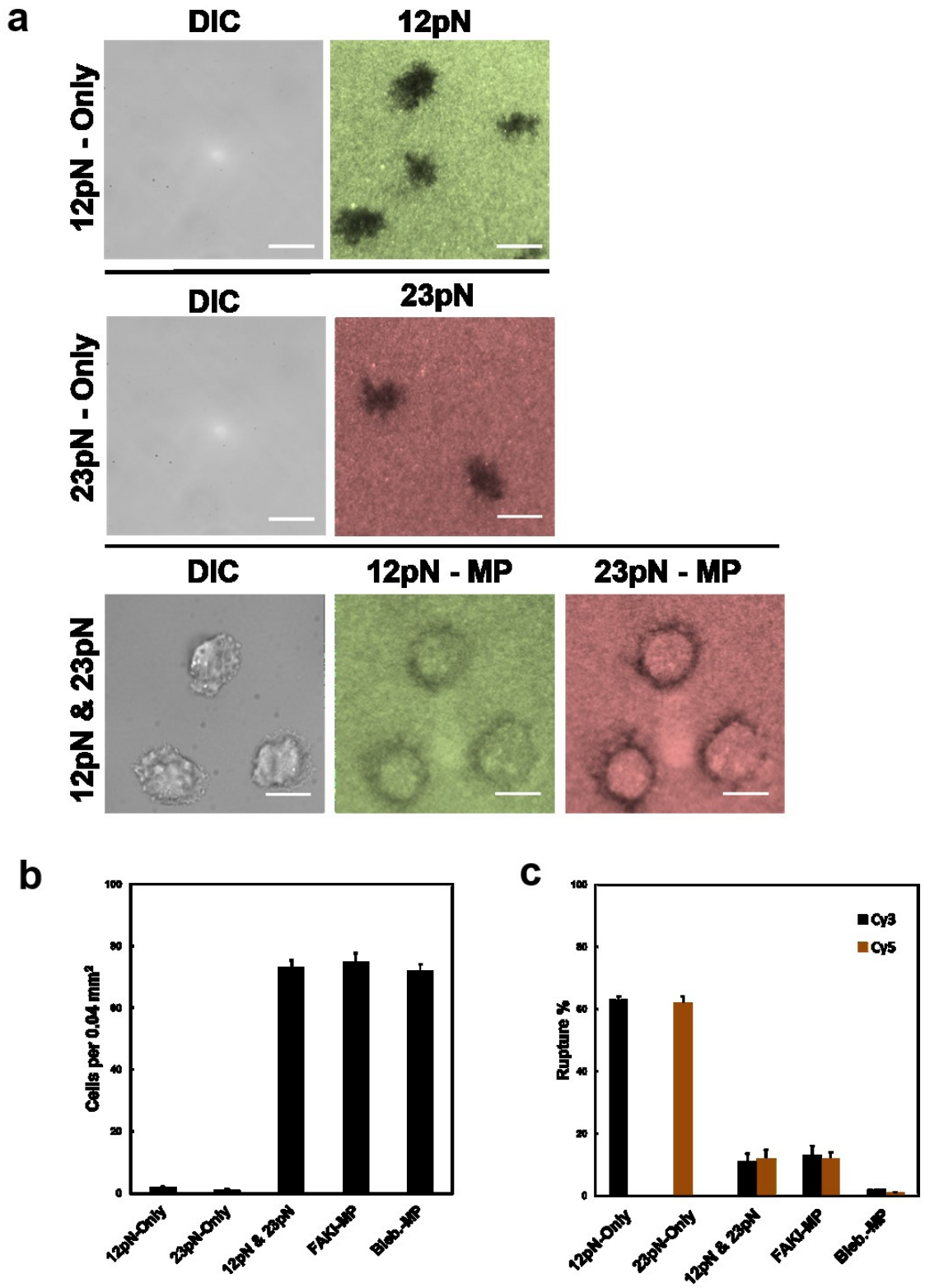
a
DIC
12pN
12pN - Only
DIC
23pN
23pN - Only
DIC
12pN - MP
23pN - MP
12pN & 23pN
b
Cells per 0.04 mm²
100
80
60
40
20
0
12pN-Only
23pN-Only
12pN & 23pN
FAK/-MP
Bleb.-MP
c
Rupture %
Cy3
Cy5
100
80
60
40
20
0
12pN-Only
23pN-Only
12pN & 23pN
FAK/-MP
Bleb.-MP

Figure 2. 2

Figure 2. 2: Reaction of cells to mechanically homogeneous surface with only one type of TGT (12 pN-Only or 23 pN-Only) and mechanically heterogeneous surface with multiplexing two different types of TGTs (12 pN or 23 pN). (a) Differential image contrast (DIC) images with 100X magnification show that cells are not adhering to the '12 pN-Only' and '23 pN-Only' surfaces. However, cells adhere to the surface covered with multiplexing of 12 pN and 23 pN TGTs ("12 pN & 23 pN"). Fluorescent footprint of cells in mechanically homogeneous environment (either 12 pN-Only or 23 pN-Only) shows a uniform rupture of TGT beneath the cells that are already rinsed away. However, fluorescent footprint for 12 pN & 23 pN, shows the rupture is mostly at the periphery of spreading cells in both fluorescent channels of 12 pN or 23 pN TGT. Scale bars are 10 μM. (b) Number of cells adhered per area is significantly higher when the environment is mechanically heterogeneous compared to homogeneous. Adding focal adhesion kinase (FAK) inhibitor or adding myosin II inhibitor (blebbistatin) to the medium while incubating the cells on the mechanically heterogeneous surface does not inhibit cells from adhering. (c) Analysis of images show rupture percentage is significantly higher if the environment of the cell is mechanically homogeneous as opposed to the mechanically heterogeneous environment. Adding FAK inhibitor does not affect the rupture percentage of

cells adhered to multiplexing surface but adding blebbistatin lowers the TGT rupture.

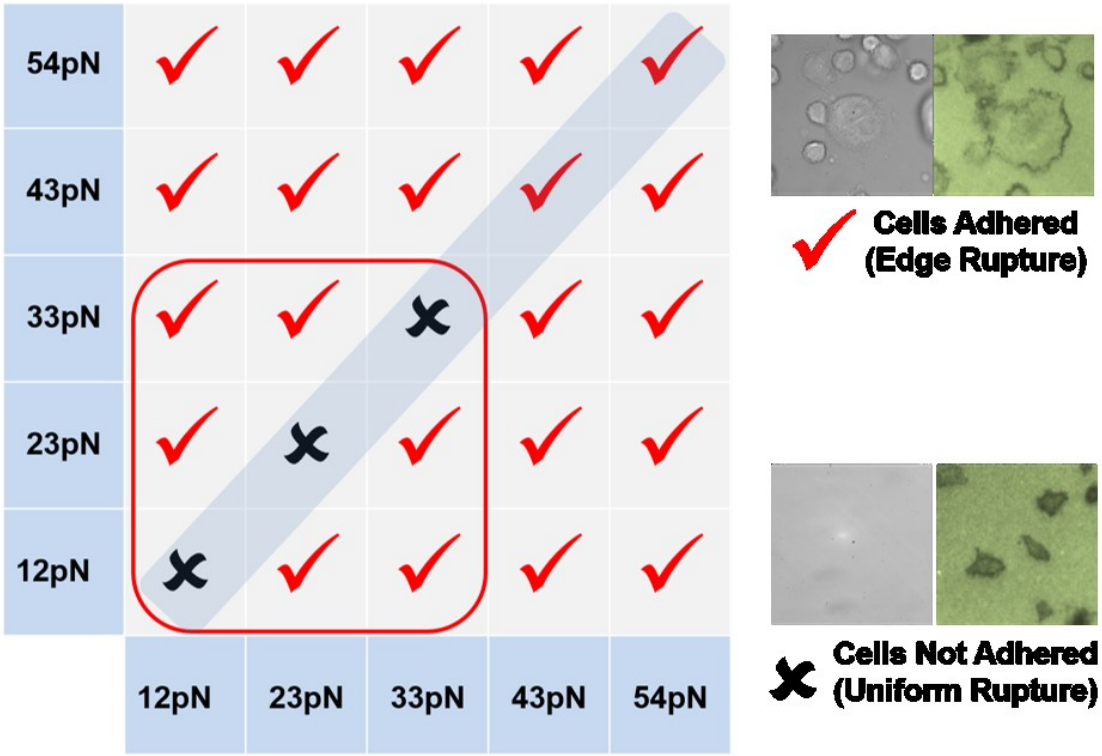
54pN
43pN
33pN
23pN
12pN
12pN
23pN
33pN
43pN
54pN
Cells Adhered
(Edge Rupture)
Cells Not Adhered
(Uniform Rupture)

Figure 2. 3

Figure 2. 3: Multiplexing TGTs with different rupture forces. The combinations out of the red box ensures cell adhesion which is trivial since at least one type of TGT is strong enough to secure the cell adhesion on its own. The diagonal combinations in the box represent a mechanically homogenous environment for cells that are too weak to allow cell adhesion. Surprisingly off diagonal combinations in the red box guarantees adhesion of cells although each TGT on its own is weak to permit cell adhesion. Note that tick mark represents cell adhesion and a fluorescent footprint with rupture at the periphery. Cross mark means lack of cell adhesion and a uniform rupture of TGT beneath the area where cell landed before detachment.

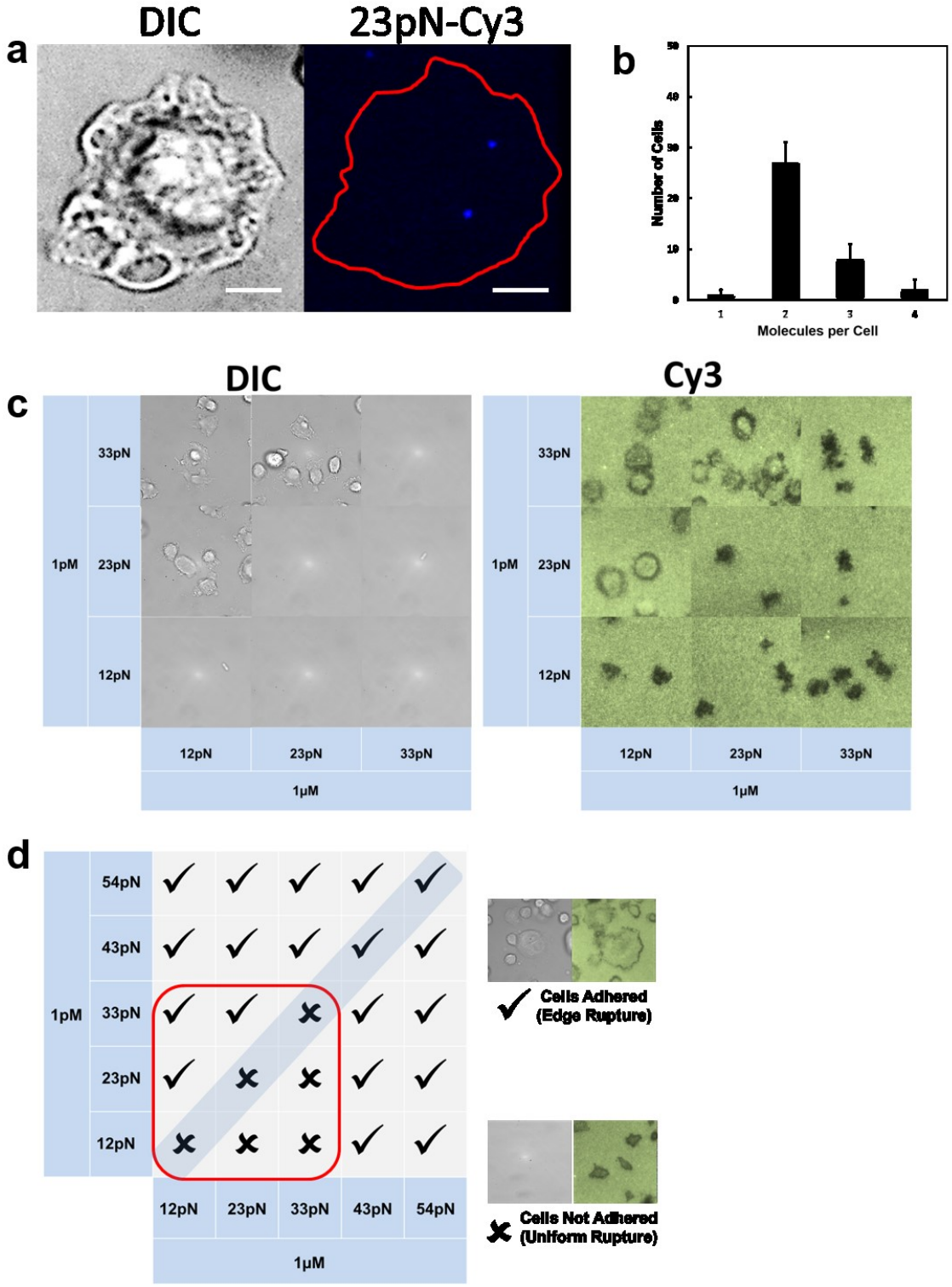
a
DIC
23pN-Cy3
b
Number of Cells
Molecules per Cell
c
DIC
Cy3
1pM
33pN
23pN
12pN
1μM
d
54pN
43pN
33pN
23pN
12pN
1pM
1μM
Cells Adhered
(Edge Rupture)
Cells Not Adhered
(Uniform Rupture)

Figure 2. 4

Figure 2. 4: Ultra-sensitivity of cells to single molecules (The Princess and The Pea or UCE). (a) The DIC image shows a cell adhered to a PnP surface (A surface covered with many weak tethers and a few tethers with relatively higher rupture force). The Cy3 image shows two single molecules of Cy3 labeled-23 pN TGT beneath the same cell in the DIC image. The incubation concentration of unlabeled-12 pN TGT and Cy3 labeled-23 pN TGT are 1 μM and 1 pM, respectively. Scale bars are 5 μm. **(b)** Number of the cells with one, two, three and four 23 pN TGT under them is shown in the same experiment as in part a. **(c)** 2-dimensional table showing the cell adhesion (left table) and fluorescent footprint of the cells (right table) for different multiplexing conditions. Concentration of TGTs are 1 pM in the vertical axis and 1 μM in the horizontal axis. Cells adhere to the surface and show edge rupture while 1 μM TGT is multiplexed with 1 pM relatively stronger TGT (upper off-diagonal conditions). If 1 μM TGT is multiplexed with 1 pM relatively weaker TGT cells do not adhere and they show entire rupture fluorescent footprint (lower off-diagonal conditions). Cells do not adhere to the diagonal conditions which imply the mechanically homogenous environment with weak tethers. **(d)** Similar table to part c with a bigger range of TGT rupture from 12 pN to 54 pN is shown. Tick mark means cells are adhered and fluorescent footprint

of the cells is rupture of tethers at the edge while cross mark means cells are not adhered and they show uniform rupture fluorescent footprint.

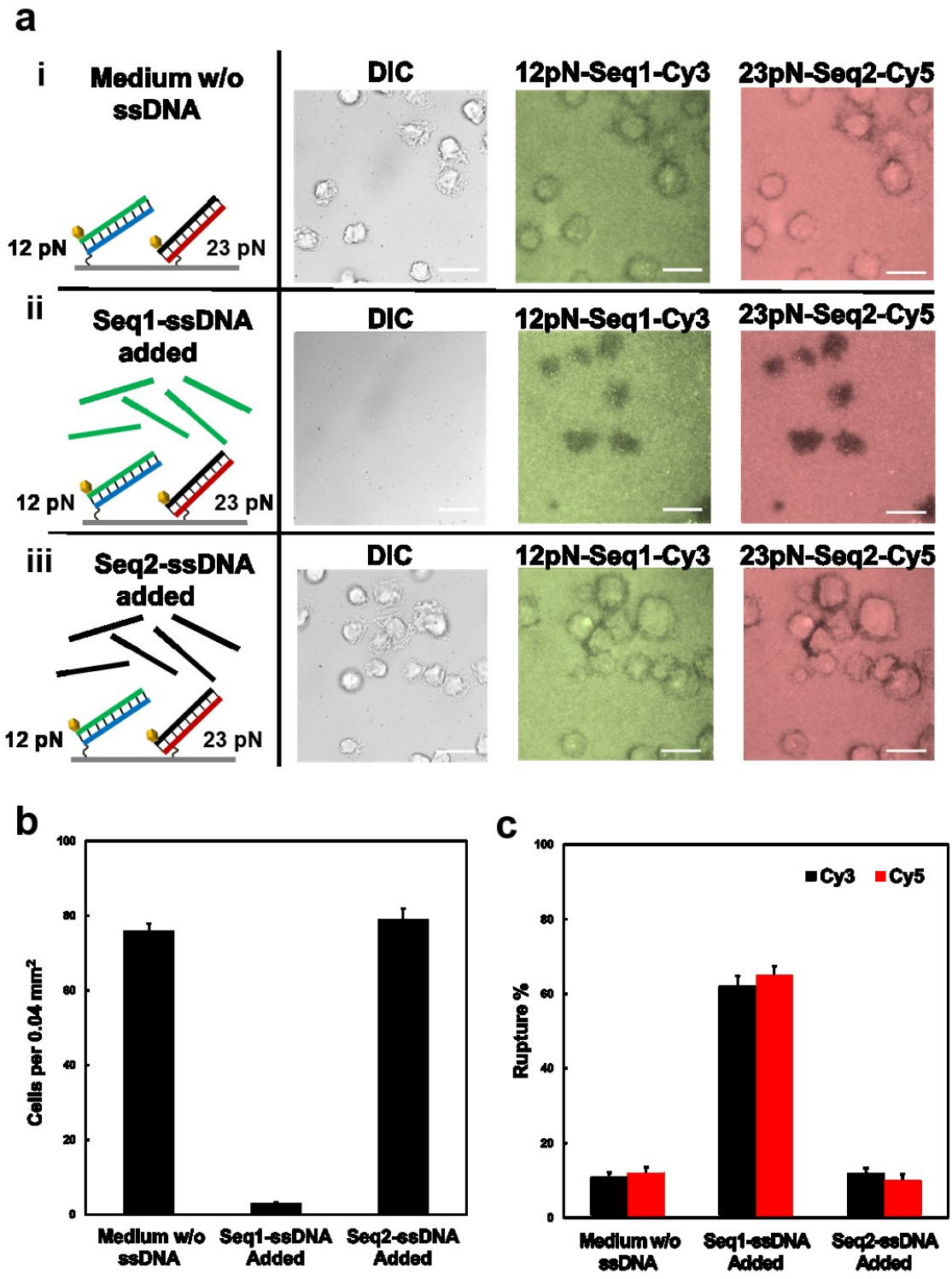
a
i
Medium w/o ssDNA
12 pN
23 pN
DIC
12pN-Seq1-Cy3
23pN-Seq2-Cy5
ii
Seq1-ssDNA added
12 pN
23 pN
DIC
12pN-Seq1-Cy3
23pN-Seq2-Cy5
iii
Seq2-ssDNA added
12 pN
23 pN
DIC
12pN-Seq1-Cy3
23pN-Seq2-Cy5
b
Cells per 0.04 mm²
0
20
40
60
80
100
Medium w/o ssDNA
Seq1-ssDNA Added
Seq2-ssDNA Added
c
Cy3
Cy5
Rupture %
0
20
40
60
80
100
Medium w/o ssDNA
Seq1-ssDNA Added
Seq2-ssDNA Added

Figure 2. 5

Figure 2. 5: Multiplexing TGT experiments with different culture medium conditions. In all the experiments 0.5 μM 12 pN TGT with sequence 1 (12 pN-Seq1-Cy3) was multiplexed with 0.5 μM 23 pN TGT with sequence 2 (23 pN-Seq2-Cy5). **(a) i)** In the normal medium without any free competitor ssDNA, cells adhered to the surface and the fluorescent footprints showed edge rupture. **ii)** Incubation of cells in a medium containing 1 μM of ssDNA with sequence 1 (upper-Seq1-ssDNA) which is the sequence for upper strand of 12 pN TGT, resulted in loss of cell adhesion to the surface. Fluorescent footprints show entire rupture. **iii)** Adding 1 μM ssDNA with the sequence 2 (upper-Seq2-ssDNA) which is the sequence for 23 pN TGT did not negatively affect cell adhesion and the fluorescent footprints are showing edge rupture. **(b)** Comparison between the numbers of adhered cells per area in the three experiments mentioned in part a shows adding ssDNA associated with the weaker tether (12 pN-Seq1-Cy3) prevents the cells from adhesion but ssDNA associated with the stronger tether (23 pN-Seq2-Cy5) does not have such an effect. **(c)** Analysis of images indicating significantly higher rupture percentage for the cell culture medium with 1 μM upper-Seq1-ssDNA compared to normal medium without any ssDNA or the medium with 1 μM upper-Seq2-ssDNA. Scale bars are 10 μM. All added ssDNAs are the upper strands of Sequence 1 and sequence 2. Adding 1 μM of lower ssDNA for

sequence 1 and sequence 2 had similar results to its respective upper ssDNA (supplementary Fig. 4).

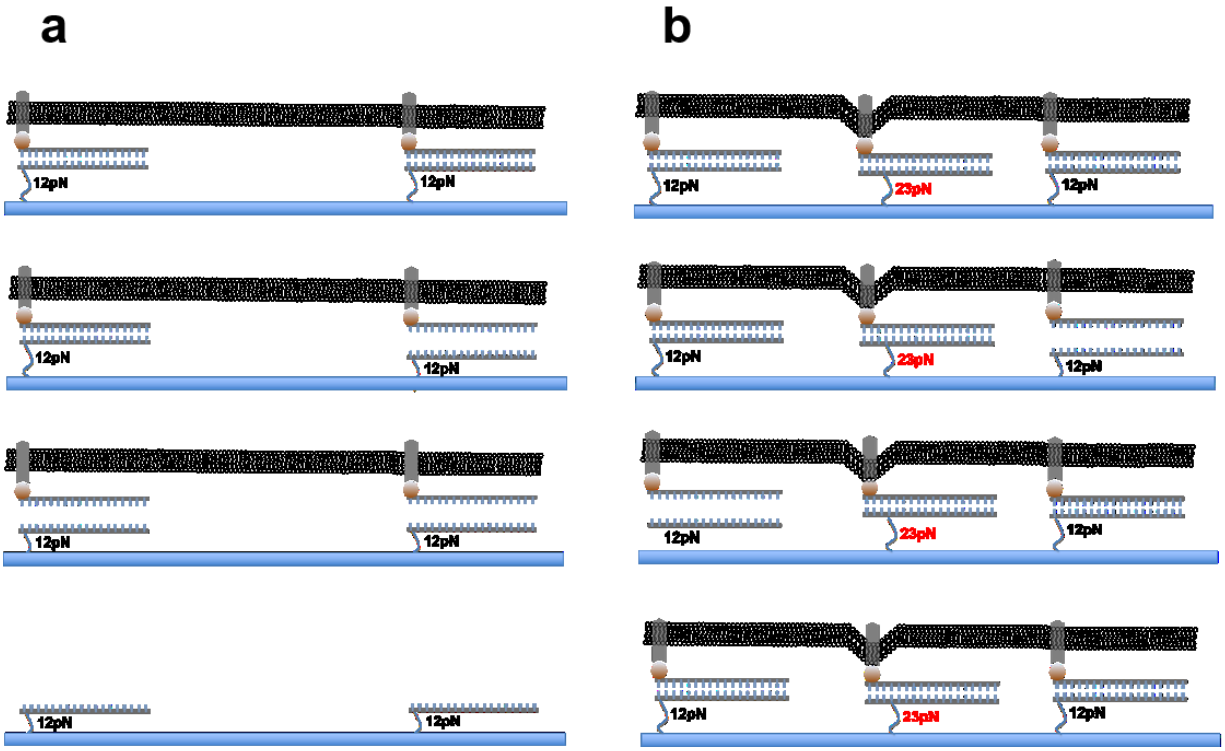
a
b
12pN
12pN
12pN
12pN
12pN
12pN
12pN
12pN
12pN
12pN
12pN
23pN
12pN
12pN
23pN
12pN
12pN
23pN
12pN
12pN
23pN
12pN

Figure 2. 6

Figure 2. 6: Schematic of membrane-holder mechanism for cell adhesion to mechanically heterogeneous surface. (a) The surface is mechanically homogeneous by covering with 12 pN TGTs. Due to undulation of the membrane, weak TGTs get ruptured and cells do not adhere to the surface. **(b)** The surface is covered with both 12 pN and 23 pN TGTs. The relatively stronger TGTs (23 pN TGTs) act as membrane holders and keep the membrane close to the surface. Partial or full rupture of the 12 pN TGTs, will be reversed since the membrane is held close to the surface due to the membrane holders (23 pN) and cells remain adhered on this surface. We found that presence of only two molecules of 23 pN TGTs per cell as membrane holders could keep the cells adhered to the surface.

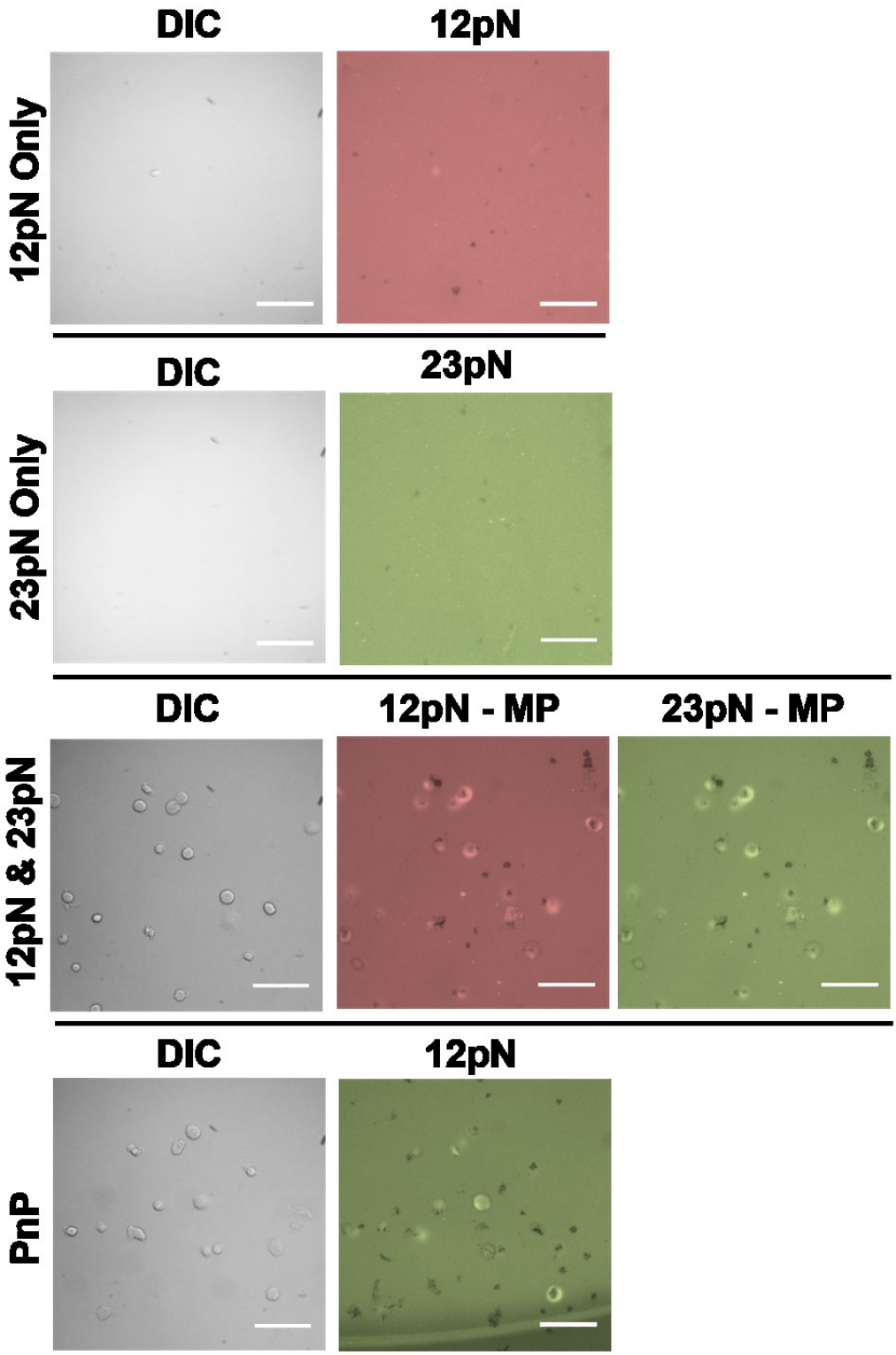

Supplementary Figure 2. 1

Supplementary Figure 2. 1: Another cell type other than CHO-K1 cells (B16-F1) with the ability of adhering to mechanically heterogeneous surface. Differential image contrast (DIC) images of B16-F1 cells show they are not adhering to the surfaces covered with either 12 pN TGT or 23 pN TGT depicted as '12 pN-only' and '23 pN-only', respectively. However, cells adhere to the surface covered with multiplexing of 12 pN and 23 pN TGTs, depicted as "12 pN & 23 pN" or the PnP surface. Fluorescent footprints of cells show the difference between mechanically homogeneous and heterogeneous environments. Scale bars are 50 μm.

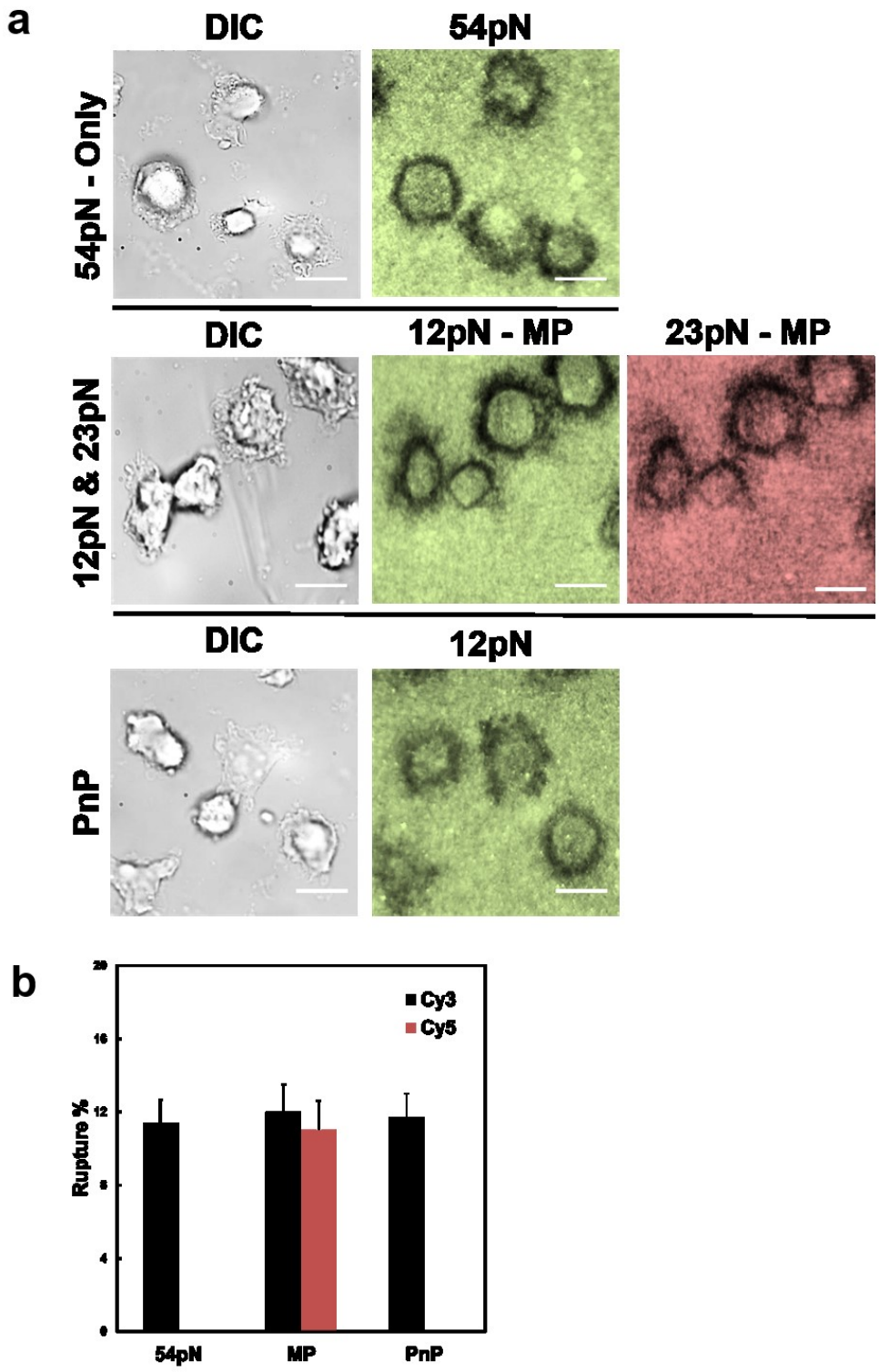

Supplementary Figure 2. 2

Supplementary Figure 2. 2: Rupture percentage of TGT and fluorescent footprint are similar for 54 surface, 12 pN & 23 pN surface and PnP surface. **(a)** DIC and fluorescent footprint images of cells on 54 surface, 12 pN & 23 pN surface and PnP surface are depicted. **(b)** Comparing rupture percentages in the fluorescent footprint of cells on the surface with 54 TGT shows similar rupture for all three surfaces. The concentration of 54 TGT incubation is 1 μM and the concentration in the multiplexing experiment is 0.5 μM for each of 12 pN and 23 pN TGT. On the PnP surface the concentration of TGT incubation is 1 μM 12 pN and 1 pM 23 pN. Scale bars are 10 μm.

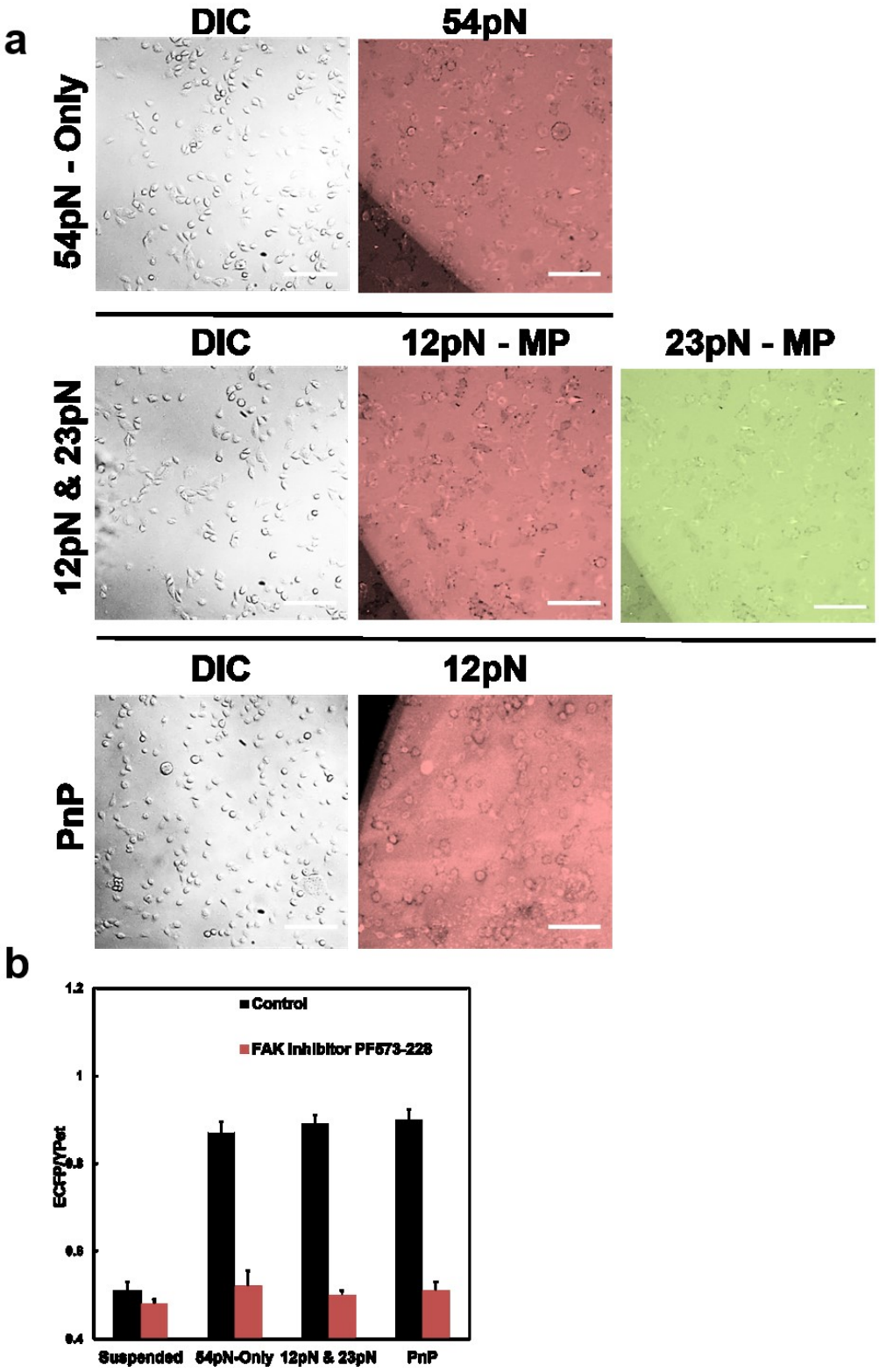

Supplementary Figure 2. 3

Supplementary Figure 2. 3: Effect of focal adhesion kinase (FAK) inhibitor (a) Applying 100 µM of FAK inhibitor PF573-228 while incubating CHO-K1 cells in 37°C did not prevent them from adhesion to 54 surface, 12 pN&23 pN surface or PnP surface. FAK inhibitor did not change footprints of the cells either. **(b)** Cytosolic FAK biosensor based on FRET was used to confirm the inhibition of FAK. Surprisingly the activity of FAK is similar in all 54, 12 pN&23 pN and PnP surface. Scale bars are 50 µm.

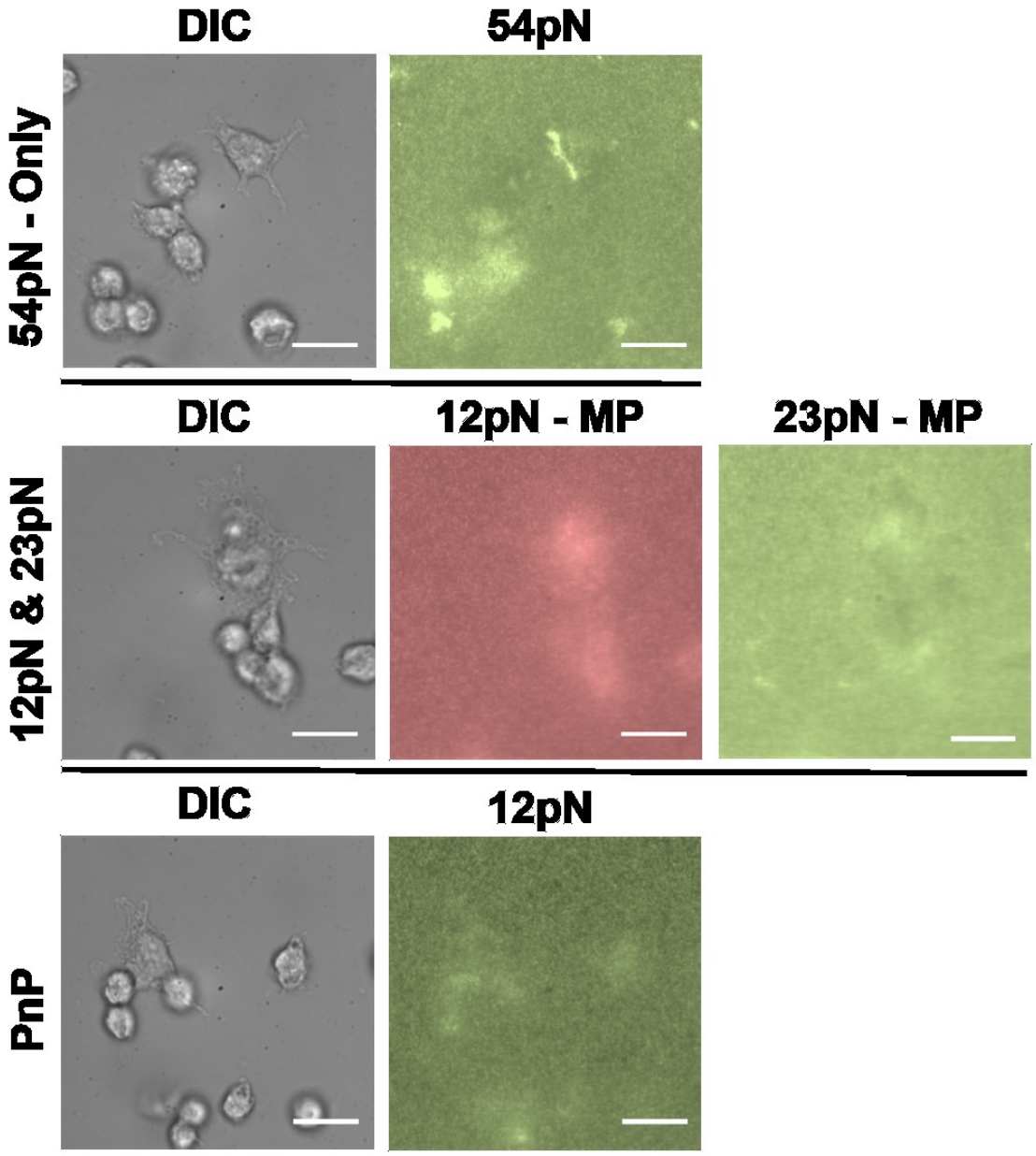

Supplementary Figure 2. 4

Supplementary Figure 2. 4: Inhibiting myosin II by adding 50 µM of blebbistatin to the medium during Incubation of CHO-K1 cells at 37°C on a surface with multiplexing of 0.5 µM of 12 pN and 0.5 µM of 23 pN TGT. The DIC images show the cells are still adhered to the 54 surface, 12 pN&23 pN surface or PnP surface. Cell adhesion during myosin II inhibition shows mysin II is not involved in the mechanism of adherence of cells to a mechanically heterogeneous surface. Note that in the fluorescent footprints of the cells there is no edge rupture, which implies the origin of the force at the periphery of CHO-K1 cells, is myosin II. Scale bars are 10 µm.

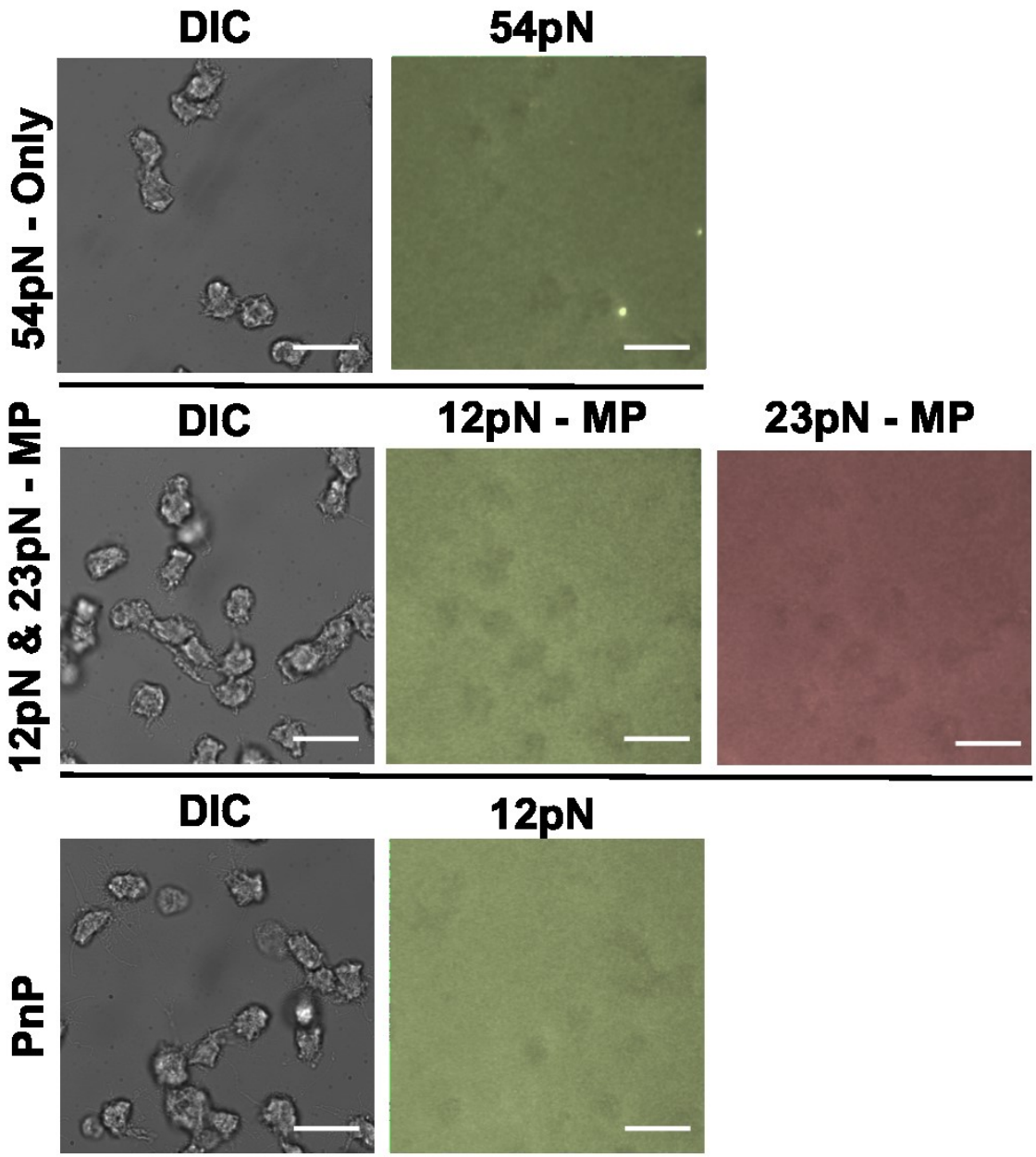

Supplementary Figure 2. 5

Supplementary Figure 2. 5: Inhibiting actin polymerization by adding latrunculin to the medium during Incubation of CHO-K1 cells at 37°C on a surface with multiplexing of 0.5 µM of 12 pN and 0.5 µM of 23 pN TGT. Cells adhere to PnP and 12 pN & 23 pN surface similar to 54 surface with a concentration of 1 µM actin inhibitor (latrunculin). The cells adhere to all three surfaces by increasing the latrunculin concentration up to 5 µM. The fluorescent footprint of the cells doesn't show the edge rupture due to the inhibition of actin polymerization. Scale bars are 10 µm.

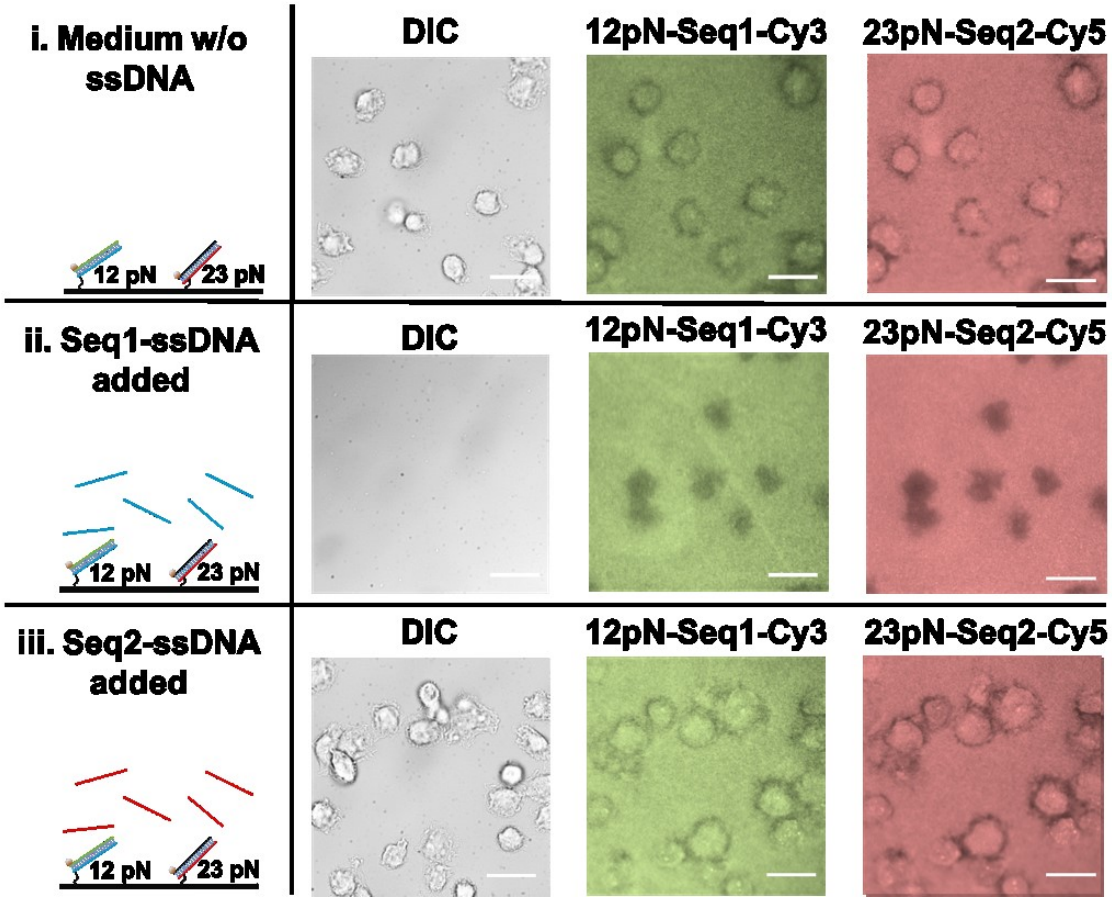

Supplementary Figure 2. 6

Supplementary Figure 2. 6: Multiplexing TGT experiments with different culture medium conditions. In all the experiments 0.5 μM 12 pN TGT with sequence 1 (12 pN-Seq1-Cy3) was multiplexed with 0.5 μM 23 pN TGT with sequence 2 (23 pN-Seq2-Cy5). This is a similar experiment to Fig. 3; however, lower ssDNA has to be added to the medium while incubation instead of upper ssDNA. **(a) i)** In the normal medium without any free competitor ssDNA, cells adhered to the surface and the fluorescent footprints showed edge rupture. **ii)** Incubation of cells in a medium containing 1 μM of lower ssDNA with sequence 1 (lower-Seq1-ssDNA) which is the sequence for upper strand of 12 pN TGT, resulted in loss of cell adhesion to the surface. Fluorescent footprints show entire rupture. **iii)** Adding 1 μM lower ssDNA with the sequence 2 (lower-Seq2-ssDNA) which is the sequence for 23 pN TGT did not negatively affect cell adhesion and the fluorescent footprints are showing edge rupture. Adding upper or lower ssDNAs for Sequence 1 and sequence 2 have similar effects in terms of number of cells adhered and the quantity of tether rupture and fluorescent footprints. Scale bars are 10 μm.

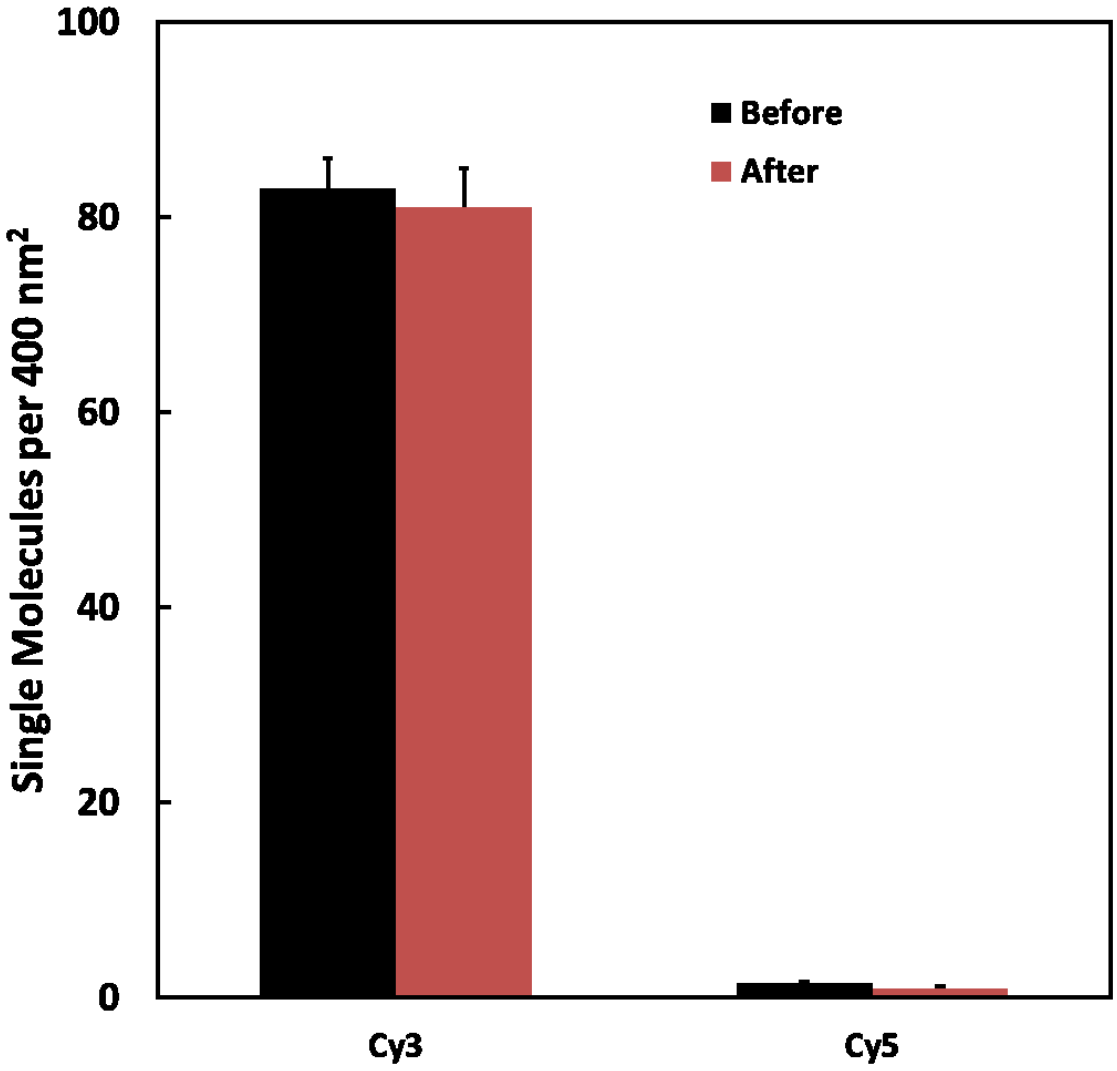

Supplementary Figure 2. 7

Supplementary Figure 2. 7: Control experiment to test whether upper ssDNA on the TGT bound to the surface could be substituted by free competitor ssDNA. Single molecules of TGT attached to the surface (with Cy3 dye) are imaged before and after 30-minute incubation in the medium with 1 μM free competitor upper ssDNA (with Cy5 dye) complementary to the TGT. Since the number of Cy5 molecules after incubation is not increased, the possibility of substitution of upper ssDNA in TGT by the free competitor ssDNA is ruled out. The surface was amply rinsed after the incubation to assure all free competitor ssDNAs in the media with Cy5 dye is washed away.

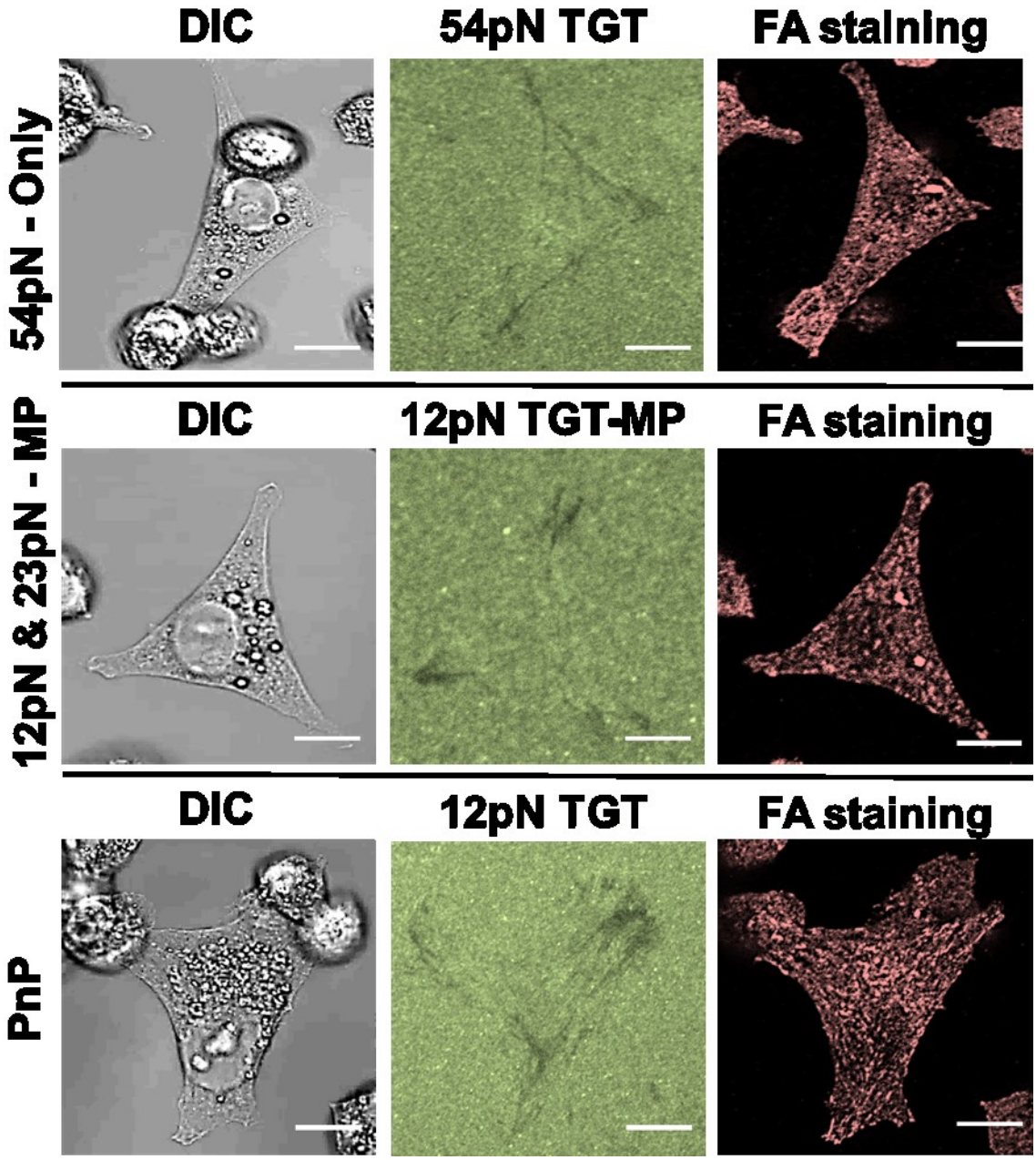

Supplementary Figure 2. 8

Supplementary Figure 2. 8: Comparing the number of focal adhesions for the cells on the surface with 54 TGT and surface with multiplexing of 12 pN and 23 pN. The images are taken by 40x confocal microscope. DIC images, fluorescent footprint of corresponding cell and focal adhesion (FA) staining of the cells are shown on 54-Only surface, 12 pN & 23 pN surface and PnP surface. Scale bar is 5 µm.

REFERENCES

Albrecht, C., Blank, K., Lalic-Multhaler, M., Hirler, S., Mai, T., Gilbert, I., Schiffmann, S., Bayer, T., Clausen-Schaumann, H., and Gaub, H. E. (2003). DNA: a programmable force sensor. *Science* **301**, 367-70.

Aumailley, M., Gurrath, M., Muller, G., Calvete, J., Timpl, R., and Kessler, H. (1991). Arg-Gly-Asp constrained within cyclic pentapeptides. Strong and selective inhibitors of cell adhesion to vitronectin and laminin fragment P1. *FEBS Lett* **291**, 50-4.

Blakely, B. L., Dumelin, C. E., Trappmann, B., McGregor, L. M., Choi, C. K., Anthony, P. C., Duesterberg, V. K., Baker, B. M., Block, S. M., Liu, D. R., and Chen, C. S. (2014). A DNA-based molecular probe for optically reporting cellular traction forces. *Nat Methods*.

Bonnans, C., Chou, J., and Werb, Z. (2014). Remodelling the extracellular matrix in development and disease. *Nat Rev Mol Cell Biol* **15**, 786-801.

Bruinsma, R., Behrisch, A., and Sackmann, E. (2000). Adhesive switching of membranes: experiment and theory. *Phys Rev E Stat Phys Plasmas Fluids Relat Interdiscip Topics* **61**, 4253-67.

Cavalcanti-Adam, E. A., Volberg, T., Micoulet, A., Kessler, H., Geiger, B., and Spatz, J. P. (2007). Cell spreading and focal adhesion dynamics are regulated by spacing of integrin ligands. *Biophys J* **92**, 2964-74.

Chan, C. E., and Odde, D. J. (2008). Traction dynamics of filopodia on compliant substrates. *Science* **322**, 1687-91.

Chiquet, M., Gelman, L., Lutz, R., and Maier, S. (2009). From mechanotransduction to extracellular matrix gene expression in fibroblasts. *Biochim Biophys Acta* **1793**, 911-20.

Chowdhury, F., Li, I. T., Leslie, B. J., Doganay, S., Singh, R., Wang, X., Seong, J., Lee, S. H., Park, S., Wang, N., and Ha, T. (2015). Single molecular force across single integrins dictates cell spreading. *Integr Biol (Camb)*.

Cocco, S., Monasson, R., and Marko, J. F. (2001). Force and kinetic barriers to unzipping of the DNA double helix. *Proc Natl Acad Sci U S A* **98**, 8608-13.

de Gennes, P. G. (2008). Maximum pull out force on DNA hybrids. *In* "arXiv:physics/0110011v1".

del Rio, A., Perez-Jimenez, R., Liu, R., Roca-Cusachs, P., Fernandez, J. M., and Sheetz, M. P. (2009). Stretching single talin rod molecules activates vinculin binding. *Science* **323**, 638-41.

Discher, D. E., Janmey, P., and Wang, Y. L. (2005). Tissue cells feel and respond to the stiffness of their substrate. *Science* **310**, 1139-43.

Dobereiner, H. G., Dubin-Thaler, B., Giannone, G., Xenias, H. S., and Sheetz, M. P. (2004). Dynamic phase transitions in cell spreading. *Phys Rev Lett* **93**, 108105.

Du, J., Chen, X. F., Liang, X. D., Zhang, G. Y., Xu, J., He, L. R., Zhan, Q. Y., Feng, X. Q., Chien, S., and Yang, C. (2011). Integrin activation and internalization on soft ECM as a mechanism of induction of stem cell differentiation by ECM elasticity. *Proceedings of the National Academy of Sciences of the United States of America* **108**, 9466-9471.

Dubin-Thaler, B. J., Giannone, G., Dobereiner, H. G., and Sheetz, M. P. (2004). Nanometer analysis of cell spreading on matrix-coated surfaces reveals two distinct cell states and STEPs. *Biophys J* **86**, 1794-806.

Dubin-Thaler, B. J., Hofman, J. M., Cai, Y., Xenias, H., Spielman, I., Shneidman, A. V., David, L. A., Dobereiner, H. G., Wiggins, C. H., and Sheetz, M. P. (2008). Quantification of cell edge velocities and traction forces reveals distinct motility modules during cell spreading. *PLoS ONE* **3**, e3735.

Elosegui-Artola, A., Bazellieres, E., Allen, M. D., Andreu, I., Oria, R., Sunyer, R., Gomm, J. J., Marshall, J. F., Jones, J. L., Trepat, X., and Roca-Cusachs, P. (2014a). Rigidity sensing and adaptation through regulation of integrin types. *Nature Materials* **13**, 631-637.

Elosegui-Artola, A., Bazellieres, E., Allen, M. D., Andreu, I., Oria, R., Sunyer, R., Gomm, J. J., Marshall, J. F., Jones, J. L., Trepat, X., and Roca-Cusachs, P. (2014b). Rigidity sensing and adaptation through regulation of integrin types. *Nat Mater* **13**, 631-7.

Engler, A. J., Sen, S., Sweeney, H. L., and Discher, D. E. (2006). Matrix elasticity directs stem cell lineage specification. *Cell* **126**, 677-89.

Evans, E. A., and Calderwood, D. A. (2007). Forces and bond dynamics in cell adhesion. *Science* **316**, 1148-53.

Fraley, S. I., Feng, Y. F., Krishnamurthy, R., Kim, D. H., Celedon, A., Longmore, G. D., and Wirtz, D. (2010). A distinctive role for focal adhesion proteins in three-dimensional cell motility. *Nature Cell Biology* **12**, 598-U169.

Friedland, J. C., Lee, M. H., and Boettiger, D. (2009). Mechanically activated integrin switch controls alpha5beta1 function. *Science* **323**, 642-4.

Geiger, B., Spatz, J. P., and Bershadsky, A. D. (2009). Environmental sensing through focal adhesions. *Nat Rev Mol Cell Biol* **10**, 21-33.

Geiger, B., and Yamada, K. M. (2011). Molecular architecture and function of matrix adhesions. *Cold Spring Harb Perspect Biol* **3**.

Ghassemi, S., Meacci, G., Liu, S., Gondarenko, A. A., Mathur, A., Roca-Cusachs, P., Sheetz, M. P., and Hone, J. (2012). Cells test substrate rigidity by local contractions on submicrometer pillars. *Proc Natl Acad Sci U S A* **109**, 5328-33.

Giannone, G., Dubin-Thaler, B. J., Dobereiner, H. G., Kieffer, N., Bresnick, A. R., and Sheetz, M. P. (2004). Periodic lamellipodial contractions correlate with rearward actin waves. *Cell* **116**, 431-43.

Gordon, W. R., Zimmerman, B., He, L., Miles, L. J., Huang, J., Tiyanont, K., McArthur, D. G., Aster, J. C., Perrimon, N., Loparo, J. J., and Blacklow, S. C. (2015). Mechanical Allostery: Evidence for a Force Requirement in the Proteolytic Activation of Notch. *Dev Cell* **33**, 729-36.

Grashoff, C., Hoffman, B. D., Brenner, M. D., Zhou, R., Parsons, M., Yang, M. T., McLean, M. A., Sligar, S. G., Chen, C. S., Ha, T., and Schwartz, M. A. (2010). Measuring mechanical tension across vinculin reveals regulation of focal adhesion dynamics. *Nature* **466**, 263-6.

Guan, J. L. (1997). Role of focal adhesion kinase in integrin signaling. *Int J Biochem Cell Biol* **29**, 1085-96.

Gurrath, M., Muller, G., Kessler, H., Aumailley, M., and Timpl, R. (1992). Conformation/activity studies of rationally designed potent anti-adhesive RGD peptides. *Eur J Biochem* **210**, 911-21.

Halder, G., Dupont, S., and Piccolo, S. (2012). Transduction of mechanical and cytoskeletal cues by YAP and TAZ. *Nat Rev Mol Cell Biol* **13**, 591-600.

Hall, A. (1998). Rho GTPases and the actin cytoskeleton. *Science* **279**, 509-14.

Hatch, K., Danilowicz, C., Coljee, V., and Prentiss, M. (2008). Demonstration that the shear force required to separate short double-stranded DNA does not increase significantly with sequence length for sequences longer than 25 base pairs. *Phys Rev E Stat Nonlin Soft Matter Phys* **78**, 011920.

Hoffman, B. D., Grashoff, C., and Schwartz, M. A. (2011). Dynamic molecular processes mediate cellular mechanotransduction. *Nature* **475**, 316-23.

Ingber, D. E. (2006). Cellular mechanotransduction: putting all the pieces together again. *FASEB J* **20**, 811-27.

Jiang, G., Giannone, G., Critchley, D. R., Fukumoto, E., and Sheetz, M. P. (2003). Two-piconewton slip bond between fibronectin and the cytoskeleton depends on talin. *Nature* **424**, 334-7.

Jurchenko, C., Chang, Y., Narui, Y., Zhang, Y., and Salaita, K. S. (2014). Integrin-generated forces lead to streptavidin-biotin unbinding in cellular adhesions. *Biophys J* **106**, 1436-46.

Kim, J., Hudson, N. E., and Springer, T. A. (2015). Force-induced on-rate switching and modulation by mutations in gain-of-function von Willebrand diseases. *Proc Natl Acad Sci U S A* **112**, 4648-53.

Koo, L. Y., Irvine, D. J., Mayes, A. M., Lauffenburger, D. A., and Griffith, L. G. (2002). Co-regulation of cell adhesion by nanoscale RGD organization and mechanical stimulus. *J Cell Sci* **115**, 1423-33.

Kumar, S., and Weaver, V. M. (2009). Mechanics, malignancy, and metastasis: the force journey of a tumor cell. *Cancer Metastasis Rev* **28**, 113-27.

Lehenkari, P. P., and Horton, M. A. (1999). Single integrin molecule adhesion forces in intact cells measured by atomic force microscopy. *Biochem Biophys Res Commun* **259**, 645-50.

Liu, B., Chen, W., and Zhu, C. (2015). Molecular force spectroscopy on cells. *Annu Rev Phys Chem* **66**, 427-51.

Liu, Y., Yehl, K., Narui, Y., and Salaita, K. (2013). Tension sensing nanoparticles for mechano-imaging at the living/nonliving interface. *J Am Chem Soc* **135**, 5320-3.

McBeath, R., Pirone, D. M., Nelson, C. M., Bhadriraju, K., and Chen, C. S. (2004). Cell shape, cytoskeletal tension, and RhoA regulate stem cell lineage commitment. *Dev Cell* **6**, 483-95.

Mitra, S. K., and Schlaepfer, D. D. (2006). Integrin-regulated FAK-Src signaling in normal and cancer cells. *Curr Opin Cell Biol* **18**, 516-23.

Morimatsu, M., Mekhdjian, A. H., Adhikari, A. S., and Dunn, A. R. (2013). Molecular tension sensors report forces generated by single integrin molecules in living cells. *Nano Lett* **13**, 3985-9.

Morimatsu, M., Mekhdjian, A. H., Chang, A. C., Tan, S. J., and Dunn, A. R. (2015). Visualizing the interior architecture of focal adhesions with high-resolution traction maps. *Nano Lett* **15**, 2220-8.

Nobes, C. D., and Hall, A. (1995). Rho, rac, and cdc42 GTPases regulate the assembly of multimolecular focal complexes associated with actin stress fibers, lamellipodia, and filopodia. *Cell* **81**, 53-62.

Oakes, P. W., and Gardel, M. L. (2014). Stressing the limits of focal adhesion mechanosensitivity. *Curr Opin Cell Biol* **30**, 68-73.

Parsons, J. T., Horwitz, A. R., and Schwartz, M. A. (2010). Cell adhesion: integrating cytoskeletal dynamics and cellular tension. *Nature Reviews Molecular Cell Biology* **11**, 633-643.

Paszek, M. J., DuFort, C. C., Rossier, O., Bainer, R., Mouw, J. K., Godula, K., Hudak, J. E., Lakins, J. N., Wijekoon, A. C., Cassereau, L., Rubashkin, M. G., Magbanua, M. J., Thorn, K. S., Davidson, M. W., Rugo, H. S., Park, J. W., Hammer, D. A., Giannone, G., Bertozzi, C. R., and Weaver, V. M. (2014). The cancer glycocalyx mechanically primes integrin-mediated growth and survival. *Nature* **511**, 319-+.

Pfaff, M., Tangemann, K., Muller, B., Gurrath, M., Muller, G., Kessler, H., Timpl, R., and Engel, J. (1994). Selective recognition of cyclic RGD peptides of NMR defined

conformation by alpha IIb beta 3, alpha V beta 3, and alpha 5 beta 1 integrins. *J Biol Chem* **269**, 20233-8.

Pierres, A., Monnet-Corti, V., Benoliel, A. M., and Bongrand, P. (2009). Do membrane undulations help cells probe the world? *Trends Cell Biol* **19**, 428-33.

Plotnikov, S. V., Pasapera, A. M., Sabass, B., and Waterman, C. M. (2012). Force fluctuations within focal adhesions mediate ECM-rigidity sensing to guide directed cell migration. *Cell* **151**, 1513-27.

Roein-Peikar, M., Xu, Q., Wang, X., and Ha, T. Ultrasensitivity of cell adhesion to the presence of mechanically strong ligands. *(Accepted to 'Phys. Rev. X')*.

Roein-Peikar, M., Xu, Q., Wang, X. F., and Ha, T. (2016). Ultrasensitivity of Cell Adhesion to the Presence of Mechanically Strong Ligands. *Physical Review X* **6**.

Rognoni, L., Stigler, J., Pelz, B., Ylanne, J., and Rief, M. (2012). Dynamic force sensing of filamin revealed in single-molecule experiments. *Proc Natl Acad Sci U S A* **109**, 19679-84.

Sackmann, E., and Smith, A. S. (2014). Physics of cell adhesion: some lessons from cell-mimetic systems. *Soft Matter* **10**, 1644-59.

Sawada, Y., Tamada, M., Dubin-Thaler, B. J., Cherniavskaya, O., Sakai, R., Tanaka, S., and Sheetz, M. P. (2006). Force sensing by mechanical extension of the Src family kinase substrate p130Cas. *Cell* **127**, 1015-26.

Schwartz, M. A. (2010). Integrins and extracellular matrix in mechanotransduction. *Cold Spring Harb Perspect Biol* **2**, a005066.

Seong, J., Ouyang, M., Kim, T., Sun, J., Wen, P. C., Lu, S., Zhuo, Y., Llewellyn, N. M., Schlaepfer, D. D., Guan, J. L., Chien, S., and Wang, Y. (2011). Detection of focal adhesion kinase activation at membrane microdomains by fluorescence resonance energy transfer. *Nat Commun* **2**, 406.

Stabley, D. R., Jurchenko, C., Marshall, S. S., and Salaita, K. S. (2012). Visualizing mechanical tension across membrane receptors with a fluorescent sensor. *Nat Methods* **9**, 64-7.

Takada, Y., Ye, X., and Simon, S. (2007). The integrins. *Genome Biol* **8**, 215.

Tan, J. L., Tien, J., Pirone, D. M., Gray, D. S., Bhadriraju, K., and Chen, C. S. (2003). Cells lying on a bed of microneedles: an approach to isolate mechanical force. *Proc Natl Acad Sci U S A* **100**, 1484-9.

Trappmann, B., Gautrot, J. E., Connelly, J. T., Strange, D. G., Li, Y., Oyen, M. L., Cohen Stuart, M. A., Boehm, H., Li, B., Vogel, V., Spatz, J. P., Watt, F. M., and Huck, W. T. (2012). Extracellular-matrix tethering regulates stem-cell fate. *Nat Mater* **11**, 642-9.

Wan, Z., Chen, X., Chen, H., Ji, Q., Chen, Y., Wang, J., Cao, Y., Wang, F., Lou, J., Tang, Z., and Liu, W. (2015). The activation of IgM- or isotype-switched IgG- and IgE-BCR exhibits distinct mechanical force sensitivity and threshold. *Elife* **4**.

Wang, N., Butler, J. P., and Ingber, D. E. (1993). Mechanotransduction across the cell surface and through the cytoskeleton. *Science* **260**, 1124-7.

Wang, X., and Ha, T. (2013). Defining single molecular forces required to activate integrin and notch signaling. *Science* **340**, 991-4.

Wang, X., Sun, J., Xu, Q., Chowdhury, F., Roein-Peikar, M., Wang, Y., and Ha, T. (2015a). Integrin Molecular Tension within Motile Focal Adhesions. *Biophys J* **109**, 2259-67.

Wang, X. F., Sun, J., Xu, Q., Chowdhury, F., Roein-Peikar, M., Wang, Y. X., and Ha, T. (2015b). Integrin Molecular Tension within Motile Focal Adhesions. *Biophysical Journal* **109**, 2259-2267.

Wang, Y., Botvinick, E. L., Zhao, Y., Berns, M. W., Usami, S., Tsien, R. Y., and Chien, S. (2005). Visualizing the mechanical activation of Src. *Nature* **434**, 1040-5.

Watt, F. M., and Huck, W. T. (2013). Role of the extracellular matrix in regulating stem cell fate. *Nat Rev Mol Cell Biol* **14**, 467-73.

Wegener, K. L., Partridge, A. W., Han, J., Pickford, A. R., Liddington, R. C., Ginsberg, M. H., and Campbell, I. D. (2007). Structural basis of integrin activation by talin. *Cell* **128**, 171-82.

Wen, J. H., Vincent, L. G., Fuhrmann, A., Choi, Y. S., Hribar, K. C., Taylor-Weiner, H., Chen, S., and Engler, A. J. (2014). Interplay of matrix stiffness and protein tethering in stem cell differentiation. *Nat Mater* **13**, 979-87.

Wiseman, P. W., Brown, C. M., Webb, D. J., Hebert, B., Johnson, N. L., Squier, J. A., Ellisman, M. H., and Horwitz, A. F. (2004). Spatial mapping of integrin interactions and dynamics during cell migration by image correlation microscopy. *J Cell Sci* **117**, 5521-34.

Wozniak, M. A., and Chen, C. S. (2009). Mechanotransduction in development: a growing role for contractility. *Nat Rev Mol Cell Biol* **10**, 34-43.

Yao, M., Goult, B. T., Chen, H., Cong, P., Sheetz, M. P., and Yan, J. (2014). Mechanical activation of vinculin binding to talin locks talin in an unfolded conformation. *Sci Rep* **4**, 4610.

Yu, C. H., Law, J. B., Suryana, M., Low, H. Y., and Sheetz, M. P. (2011a). Early integrin binding to Arg-Gly-Asp peptide activates actin polymerization and contractile movement that stimulates outward translocation. *Proc Natl Acad Sci U S A* **108**, 20585-90.

Yu, C. H., Law, J. B. K., Suryana, M., Low, H. Y., and Sheetz, M. P. (2011b). Early integrin binding to Arg-Gly-Asp peptide activates actin polymerization and contractile movement that stimulates outward translocation. *Proceedings of the National Academy of Sciences of the United States of America* **108**, 20585-20590.

Yu, C. H., Rafiq, N. B., Krishnasamy, A., Hartman, K. L., Jones, G. E., Bershadsky, A. D., and Sheetz, M. P. (2013a). Integrin-matrix clusters form podosome-like adhesions in the absence of traction forces. *Cell Rep* **5**, 1456-68.

Yu, C. H., Rafiq, N. B. M., Krishnasamy, A., Hartman, K. L., Jones, G. E., Bershadsky, A. D., and Sheetz, M. P. (2013b). Integrin-Matrix Clusters Form Podosome-like Adhesions in the Absence of Traction Forces. *Cell Reports* **5**, 1456-1468.

Yuri Sykulev, M. J., Irina Vturina, Theodore J. Tsomides, Herman N. Eisen (1996). Evidence that a Single Peptide–MHC Complex on a Target Cell Can Elicit a Cytolytic T Cell Response. *Immunity* **4**, 565-571.

Zhang, Y., Ge, C. H., Zhu, C., and Salaita, K. (2014). DNA-based digital tension probes reveal integrin forces during early cell adhesion. *Nature Communications* **5**.

CURRICULUM VITAE

Name: Mehdi Roein-Peikar

Address: 331 E University Pkwy

Baltimore, MD, 21218

E-mail: mroeinp1@jhmi.edu

Education

2015-2016 Ph.D. Candidate, Johns Hopkins School of Medicine, Department of Biophysics and Biophysical Chemistry.

2012- 2015 M.Sc., University of Illinois at Urbana-Champaign (UIUC), Physics Department.

2007- 2010 Residency in Orthodontics, Shiraz University of Medical Sciences, Shiraz, Iran.

2001- 2007 Doctorate of Dental Surgery, Shahid Beheshti University of Medical Sciences, Tehran, Iran.

Teaching Experience:

2013 **Teaching Assistant,** Ranked as Outstanding TA, UIUC Physics Department

2012 **Teaching Assistant,** Ranked as Excellent TA, UIUC Physics Department

2010- 2011 **Assistant Professor**, Shiraz University of Medical Sciences, Department of Orthodontics

Peer-Reviewed Publications:

Roein-Peikar, Mehdi, Qian Xu, Xuefeng Wang, and Taekjip Ha. "Ultrasensitivity of Cell Adhesion to the Presence of Mechanically Strong Ligands." *Physical Review X* 6, no. 1 (2016): 011001.

Lee, Min Kyung, Jooyeon Park, Xuefeng Wang, **Mehdi Roein-Peikar**, Eunkyung Ko, Ellen Qin, Jonghwi Lee, Taekjip Ha, and Hyunjoon Kong. "Rupture force of cell adhesion ligand tethers modulates biological activities of a cell-laden hydrogel." *Chemical Communications* (2016).

Wang, X., Sun, J., Xu, Q., Chowdhury, F., **Roein-Peikar, M.**, Wang, Y., & Ha, T. (2015). Integrin Molecular Tension within Motile Focal Adhesions. Biophysical Journal, 109(11), 2259-2267.

Oshagh, M.; Danaei, S. M.; Sardarian, A.; Alipour, A.; **Roein-Peikar, M.**; Khaksar, Y."Root Parallelism of Canine and Second Premolar in Preadjusted

and Standard Edgewise Systems: A Comparative Study." *Galen Medical Journal* 3.3 (2014).

Zahed, M.; MomeniDanaei, S.; Oshagh, M.; **Roein-Peikar, M.** "A Comparison of Apical Root Resorption in Incisors After Fixed Orthodontic Treatment with Standard Edgewise and Straight wire (MBT) Method", International *Journal of Dental Clinics*. 2013.

Salehi, P.; Zarif H.; **Roein-Peikar M.**; "Comparison of Survival Time between Two Types of Orthodontic Fixed Retainers: a Prospective Randomized Clinical Trial", *Progress in Orthodontics*. 2013.

Oshagh, M.; Aleyasin, Z.; **Roein-Peikar, M.** "The Effect of Forehead and Neck Position in Profile Esthetics" *European Journal of Esthetic Dentistry* 7(4):454-466.

Momeni Danaei, S.; Safavi, A.; **Roein-Peikar, M.**; Oshagh, M.; Iranpoor, S.; Omidkhoda, S.M. "Ion Release from Orthodontic Brackets in Three Different Mouthwashes - In Vitro Study", *American Journal of Orthodontics & Dentofacial Orthopedics* (AJO)-2011, 730-734.

Salehi, P.; **Roein-Peikar, M.**; Davari, M.; Emami, Z.; ZarifNajafi, H."Prediction of Mesiodistal Width of Unerrupted Canines and Premolars in

South Iranian Population with Presenting New Regression Equations" *Journal of Dental Medicine-Tehran University of Medical Sciences*. 2010, 23(2), 6-11.

Roein-Peikar, M.; Salehi, P.; Emami, Z.; Davari, M.; ZarifNajafi, H. "Evaluation of Simple Method to Predict the Anterior and Overall Bolton Discrepancy in a South Iranian Population" *Journal of Mashhad Dental School.* 2010, 34(3), 209-18.

Salehi, P.; Pakshir, H.M; **Roein-Peikar, M.**; Emami, Z.; Davari, M. "Evaluating the Accuracy of Moyers Prediction Tables and Tanaka-Johnston Regression Equations in a Sample of Iranian Population and Presenting New Regression Equations in Space Analysis" *Journal of Dentistry*. 2010, 12(1), 34-49.

Pakshir, H.M.; Salehi, P.; **Roein-Peikar, M.**; Emami Z. "Designing a Software for Space Analysis and Comparing the Accuracy of Tooth Measurements by Digital and Manual Methods" *Journal of Dentistry.* 2010, 12(3), 239-251.

<u>Book Chapter</u>

Book Title: Orthodontic Treatment.

Chapter title: The Use of Mini-Implants (Temporary Anchorage Devices) in Resolving Orthodontic Problems

ISBN 978-953-51-0143-7, InTech, DOI: 10.5772/33301. (2012)

Available at: http://goo.gl/BphcyU

Awards and Accomplishments:

2015 Patent for a novel technique in orthodontics

2015 NSF Innovation Corps (I-Corps) grant

2015 Edelheit Fellowship award in Biological Physics

2015 Highlighted discovery in cell.com and phys.org (The Princess and The Pea: A Story of Biomechanics)

2015 Highlighted talk in 59th Biophysical Society Meeting among more than 3000 presentations, Baltimore

2015 Referee/ Reviewer for the journal *Progress in Orthodontics*

2014 Gianturco Foundation Scholarship, Mayo Clinic

2014 Finalist of International HHMI fellowship, *Howard Hughes Medical Institute*

2013 American Physical Society DPF Meeting award for presentation at UC Santa Cruz

2012 Dean's Scholarship, Physics Department

2010 1st rank in the Clinical Iranian Board of Orthodontics, Iran

2008& 2009 Bronze and gold medals in swimming race, Olympiad of universities of medical sciences

2007 4th rank in the national entrance examination of Dentistry Specialty among about 3000 dentists, Iran

2001 9th rank in the Konkoor (entrance examination of universities) among 410,231 students

- Received appreciation from president of Iran for the rank in Konkoor

1997 Selected for National Organization for Development of Exceptional Talents (NODET), Iran

Memberships:

2015- Present Member of American Association of Orthodontists

2012- Present Member of American Biophysical Society

2012- Present Member of American Physical Society

1997- 2011 Member of National Organization for Development of Exceptional Talents (NODET), Iran

2007- 2011 Member of Iranian Orthodontic Research Center, Iran

2001- 2007 Member of executive committee in several dental conferences, Iran

2001-2011 Member of Iranian Lifeguard Federation

Presentation:

March 2016 **Biophysical Society 60th Annual Meeting, Los Angeles, CA.**

1. Ultrasensitivity of Cell Adhesion to the Differential Mechanical Cues and Requirement of Reversibility.

Feb. 2016 **Macromolecular Structure& Function Seminar, Johns Hopkins School of Medicine, Baltimore, MD.**

2. Molecular Requirements for A Pandemic Virus.

Oct. 2015 **BMES 2015 Annual Meeting, Tampa, FL.**

3. Mechanical Heterogeneity: A New Concept for Cell Adhesion.

May. 2015 **IGB Fellows Symposium, UIUC, IL.**

4. A New Story in Biomechanics.

Feb. 2015 **Biophysical Society 59th Annual Meeting, Baltimore, MD.**

5. The Princess and the Pea: A Story of Biomechanics.

Nov. 2014 **CPLC Symposium, UIUC, IL.**

6. Sensitivity of Cells to Mechanical Heterogeneity.

Oct. 2014 **Individualizing Medicine Conference, Mayo Clinic, Rochester, MN.**

7. Force Spectroscopy of Single Molecule Cellular Mechanics.

Aug. 2014 **3rd Midwest Single Molecule Workshop**, **UIUC, IL.**

8. Ultra-sensitivity of Cells to their Mechanical Environment.

May 2014 **IGB Fellows Symposium, UIUC, IL.**

9. Mechanobiology of Cell Adhesion.

Aug. 2013 **Meeting of the American Physical Society, Santa-Cruz, CA.**

10. Understanding light: Why we Need a Terascale Photon Collider?

May 2010 **8th International Congress of Iranian Association of Orthodontists, Tehran/Iran.**

11. Do People with Mandibular Prognathism Have a Larger Frontal Sinus?

Jun. 2010 **1st Congress of LASER Application in Dentistry, Gilan/Iran.**

12. Applications of LASER in Orthodontics.

Nov. 2009 **9th International Congress of Iranian Association of Periodontists, Tehran/Iran.**

13. Frenectomy as a Choice of Treatment of Maxillary Midline Diastema.

Oct. 2009 **9th International Congress of Iranian Association of Prosthodontists, Mashhad/Iran.**

14. The Relationship of Orthodontics and Prosthodontics in Missing Teeth Treatment Procedures.

Aug. 2009 **12th International Congress of Iranian Association of Endodontists, Tehran/Iran.**

15. Endodontic-Orthodontic Relationship- a Review of Literature.

May 2009 **31st Asia Pacific Dental Congress 2009, Hong Kong.**

16. Is There a Relationship between Center of Cranium, Nasion and Maxillary Length?

May 2009 **7th International Congress of Iranian Association of Orthodontists, Hamadan/Iran.**

17. Changes in Maxillary and Mandibular Arch after Rapid Maxillary Expansion.
18. Facial Soft Tissue Profile Changes Following BSSO and Subcondylar Mandibular Setback.
19. Root Proximity and Root Contact during Insertion of Miniscrew for Orthodontic Anchorage.
20. Mechanical and Biological Aspects of Root Resorption.

Oct. 2009 **2nd Congress of Iranian Dental Residents, Tehran/Iran.**

21. Are the Moyer's Tables Appropriate for the Iranian Population?

22. Symmetry in Mesiodistal Width of the Tooth in Right and Left Quadrants of Jaws.

23. The Effect of Environmental Factors on Force Decay Pattern of 3 Force Delivery Systems.

May 2009 **49th Congress of Iranian Dental Association, Tehran/Iran.**

24. Periodontal Considerations for Impacted Canines in Orthodontic Patients.

Jan. 2008 **1st International Congress of Iranian Association of Maxillofacial Radiologists, Tehran/Iran.**

25. Comparing the Accuracy of Landmark Identification in Cephalograms in Digital and Manual Methods.

Nov. 2008 **8th International congress of Iranian Association of Periodontists, Kish/Iran.**

26. New Techniques of Fibrotomy to Prevent Orthodontic Relapses.

Oct. 2008 **1st Congress of Iranian Dental Residents, Hamadan/Iran.**

27. Changes in Arch Dimension after Hyrax Therapy.

Jun. 2008 **10th Congress of Iranian Dental Students, Khorasgan/Iran.**

28. Maxillary Permanent Incisors and First Molars as Predictors of Canines and Premolars Widths.

Feb. 2008 **4th International Congress of Iranian Association of OMFS, Tehran/ Iran.**

29. Orthodontic Considerations in Orthognathic Surgeries.

Jan. 2007 **6th International Congress of Iranian Association of Orthodontists, Tehran/Iran.**

30. Assessment of Hyoid Bone Position in Orthognathic Surgeries after Mandibular Setback: BSSO vs Subcondylar.

Nov.2007 **7th International Congress of Iranian Association of Operative Dentists, Shiraz/Iran.**

31. Importance of Operative Dentistry in Orthodontics (Case Report).

May 2006 **8th Congress of Iranian Dental Students, Shiraz/Iran.**

32. Prevalence of Jaw Tumors in Patients Referred to Shiraz Dental School from 1983 to 1993.

Nov. 2006 **4th International Congress of Iranian Association of Orthodontists, 2005/Shiraz-Iran.**

33. Animals in Orthodontic Researches.

Feb. 2005 **12th International Congress of Iranian Medical Students, Tabriz/Iran.**

34. Craniofacial Fibrous Dysplasia- a Case Report.

Feb. 2004 **7th Congress of Iranian Dental Students, Rafsenjan/Iran.**

35. Actinobacillus Actinomycetcomitans and its Effects on Periodontal Disease.